공학박사 학위논문

Improvement of Corrosion Resistance and Biocompatibility via Functional Surface Modification on Magnesium Implants

생분해성 마그네슘 임플란트의 기능성 표면 처리를 통한 부식 저항성 및 생체 활성도 향상

2020년 8월

서울대학교 대학원

재료공학부

천 광 희

Improvement of Corrosion Resistance and Biocompatibility via Functional Surface Modification on Magnesium Implants

생분해성 마그네슘 임플란트의 기능성 표면 처리를 통한 부식 저항성 및 생체 활성도 향상

지도교수 김 현 이

이 논문을 공학박사 학위논문으로 제출함

2020년 8월

서울대학교 대학원

재료공학부

천 광 희

천 광 희의 박사 학위논문을 인준함

2020년 8월

위 원 장 안 철 희 (인)

부위원장 김 현 이 (인)

위 원 남 기 태 (인)

위 원 한 철 민 (인)

위 원 정 현 도 (인)

Abstract

Improvement of Corrosion Resistance and Biocompatibility via Functional Surface Modification on Magnesium Implants

Kwang-Hee Cheon
Department of Materials Science and Engineering
Seoul National University

Worldwide, Magnesium (Mg) and its alloy have received considerable attentions in the biomedical fields, as increasing demands for biodegradable materials. Its by-products are non-toxic during degradation of Mg in the physiological conditions and there is no need for additional secondary removal surgery because tissue regeneration and dissolution of the implanted material are performed, simultaneously. In addition, Mg has most similar mechanical properties to the human bone among other metallic implant, which results in suppressing ‘stress shielding effect’. Despite these advantages, poor corrosion

resistance of magnesium leads to limitation of its practical use in the biomedical applications. Therefore, researches of surface treatments to augment corrosion resistance and biocompatibility of magnesium have been actively conducted. In this study, considering deformation applied to the material in the real situation, studies about the PEI-based functional coatings were performed to improve the corrosion resistance and biocompatibility under the deformation.

In the first study, hydroxyapatite (HA)-polyetherimide (PEI) coated Mg was developed on the micro-groove patterned surface of Mg, which improved the corrosion resistance, biocompatibility of magnesium in the deformed situation. Conventional bio-ceramic coatings greatly enhanced corrosion resistance and biocompatibility of magnesium, but their function could deteriorate under deformation because of their brittleness. In order to solve this problem, micro-groove pattern was introduced on the magnesium surface to control strain distribution. Firstly, the groove size was optimized using finite element analysis software by analyzing strain distribution, value and effective surface area according to various aspect ratio. Based on the results of simulation, micro-groove pattern of 20μm was fabricated uniformly by laser machining. And then HA, which has excellent biocompatibility and corrosion resistance, was coated on the hill part of the grooves where little strain occurs and PEI was coated on the valley parts of the grooves, where the strain was concentrated, through a series of coating process. It was confirmed that surface

morphology of the HA-PEI coating layer was sustained without any defects even after tensile deformation, as opposed to that of HA coating. Corrosion resistance and biocompatibility of the HA-PEI coated Mg were also maintained before and after applying deformation. Consequently, proposed ceramic-polymer coating can be adopted in various Mg based medical applications depending on their clinical use.

In the second study, tantalum (Ta) ion implanted PEI coating was obtained to achieve better biocompatibility and bioactivity with excellent flexibility and corrosion resistance of the PEI layer. Typical polymer coatings have excellent flexibility, which can be applied to many deformable biomedical devices. However, since they show low biocompatibility and bioactivity, it is necessary to improve biological properties stably. Ta, which is known as a highly bioactive material, was implanted into a PEI coating on magnesium using an ion implantation process, so called S-PIII. Ta ions were implanted into polymer matrix with a thickness of 15 nm without any interface and defects. Implanted Ta ions stably existed compared to just Ta coating even under high tensile deformation. Corrosion resistance, biocompatibility, and bioactivity of Ta/PEI-coated Mg was remarkably increased compared to the uncoated Mg. Suggested metal-polymer coating layer, showing high deformability, corrosion resistance, biocompatibility and bioactivity, was successfully achieved.

In conclusion, these studies focused on improving the corrosion

resistance and biocompatibility of magnesium implants via various surface coatings. The HA-PEI coated Mg showed better corrosion resistance even under tensile deformation by selective coating on the groove pattern. And the Ta/PEI-coated Mg maintained surface function even at high tensile strain by implanting Ta ions into the polymer coating layer, showing remarkable improvement in corrosion resistance and biocompatibility. These results suggest that this study is promising and could be widely applied to biomedical magnesium devices, such as orthopedic implants or vascular stent.

Keywords: Magnesium (Mg); Surface coating; Corrosion resistance; Finite element analysis; Groove pattering; Hydroxyapatite (HA); Polyetherimide (PEI); Tantalum (Ta); Biodegradability;

Student number: 2014-21455

Contents

List of Tables

List of Figures

Figure 2.6 XRD patterns of the HA coated Mg (black) and the HA-PEI coated Mg (red) with micropatterns

Figure 2.7 Surface morphologies of the HA and the HA-PEI coated Mg after 5% deformation. (A) HA coated Mg with flat surface, (B) HA coated Mg with micropatterns, and (C) HA-PEI coated Mg with micropatterns.

Figure 2.8 Corrosion behaviors of the bare, the HA and the HA-PEI coated Mg samples with micropatterns after immersion for 7 days in SBF at 37 °C. pH values of the samples throughout the 7-day immersion (A) before deformation and (B) after 5% deformation of the samples. Evolved H_2 gas of the samples throughout the 7-day immersion (C) before deformation and (D) after 5% deformation of the samples.

Figure 2.9 Surface morphologies of the HA and the HA-PEI coated Mg after immersion for 7 days: HA coated Mg samples (A) before deformation and (B) after deformation. HA-PEI coated Mg samples (C) before deformation and (D) after deformation.

Figure 2.10 Cell morphologies on undeformed and deformed HA and PEI/HA-coated Mg after culturing for 5 days: HA coated Mg samples (A) before deformation and (B) after 5% deformation. HA-PEI coated Mg samples (C) before deformation and (D) after 5% deformation.

Figure 3.9 (A) The graph of evolved H_2 gas amount in SBF solution of the bare Mg, the PEI- and Ta/PEI-coated Mg after immersion in SBF solution for 10 days (B) and the calculated *in vitro* corrosion rate of each Mg sample (**$p < 0.01$).

Figure 3.10 (A) 3D images of the bare, PEI- and Ta/PEI-coated Mg at 0, 3, 6, and 14 days of immersion and their (B) remaining volumes. (C) Their calculated corrosion rates. Statistical significance is indicated by *$p < 0.05$.

Figure 3.11 CLSM images of adhered MC3T3-E1 cells on the surface of (A)–(B) bare, (C)–(D) PEI-coated Mg, and (E)–(F) Ta/PEI-coated Mg after culturing for 6 and 24 h (scale bar: 100 μm).

Figure 3.12 (A) DNA amount and (B) ALP activity of MC3T3-E1 cells on the bare, PEI- and Ta/PEI-coated Mg after culturing for 1, 3, and 5 days and 10 days, respectively (*$p < 0.05$, **$p < 0.01$, ***$p < 0.005$, and ****$p < 0.001$).

Figure 3.13 Cross-sectional 2D coronal and transverse μ-CT images of each implants after implantation for four weeks, (A)-(B) bare Mg, (C)-(D) PEI-coated Mg and (E)-(F) Ta/PEI-coated Mg sample.

Figure 3.14 3D re-constructed images of bone tissue and the bare Mg, the PEI-coated Mg and the Ta/PEI-coated Mg implant after 4 weeks (gray : specimen, yellow : bone)

the PEI-coated and Ta/PEI-coated Mg with and without drug after culturing time for 3 and 6 days. (scale bar : 100μm) (B) Surface coverage rate and (C) DNA amount of endothelial cells cultured on the PEI-coated and Ta/PEI-coated Mg with and without drug (*p < 0.05, **p < 0.01, ***p < 0.005).

Figure 4.5 (A) Representative FE-SEM images of adhered platelet on the PEI-coated and Ta/PEI-coated Mg with and without drug after culturing time for 1 hour (Scale bar : 10μm). (B) Quantitative density of adhered platelet and (C) the ratio of the activated platelet cultured on the PEI-coated and Ta/PEI-coated Mg with and without drug (*p < 0.05, **p < 0.01, ***p < 0.005, ****p<0.001).

Chapter 1.

Introduction

1.1 Outline about Biodegradable medical implants

Worldwide, there is an increasing demands and attention about biomedical implants because issues or concern about health were grown as quality or span of human life increases. Therefore, many studies have been performed on their safety or effectiveness in accordance with various medical fields, such as orthopedic surgery or vascular application. So far, commercialized metallic biomaterials were permanent materials, such as titanium (Ti), cobalt-chromium (Co-Cr), stainless steel (SUS), which have good mechanical properties, high wear resistance and satisfactory biocompatibility [1]. However, these permanent implants have a disadvantage that they require unnecessary additional surgery, cost and suffering to the patient because they have to be eliminated from implantation site after completion of regeneration. Firstly, the long-term implantation of permanent metallic implants could produce additional problems by capturing the drilled hole. Secondly, 'stress shielding effect' could be caused by high Young's modulus of these permanent materials (**Figure 1.1**). During fixation of bone, applied load can be concentrated into implanted material due to higher modulus, which results in dissolving peri-implant bone tissue, ultimately leading to failure of fixation. Moreover, toxic metal ions released from permanent metallic implants can cause unexpected clinical complications or chronic inflammation in human body for a long time

[2, 3]. As alternative way to solve these problems, biodegradable implants that were degraded without toxicity in human body has been promising and attracting attention as an important field in biomedical applications. Representative biodegradable materials include natural polymers such as collagen and chitosan, and synthetic polymers, including poly (L-lactic) acid (PLLA), poly glycol acid (PGA) and polycaprolactone (PCL) [4]. In particular, synthetic biodegradable polymers have been extensively used for orthopedic fixation implants or vascular devices with FDA approval as they do not cause stress shielding effect and artefacts during radiographic imaging [5]. However, most polymer materials are inappropriate for various load-bearing applications due to relatively poor mechanical properties. Also, they are known to cause a non-infectious inflammatory reaction, which induces pathological bone resorption due to accumulation of the acidic by-products during bulk erosion. Owing to undesirable effects, clinical concerns about biodegradable polymers have been increasing [6, 7]. Recently, magnesium (Mg)-based implants have been enormously recognized as potential substitutes because they could resolve the drawbacks of current commercialized implants. Mg and its alloys have been extensively used as orthopedic implant, such as bone plate, screw, or vascular stent since they can be degraded without toxic by-products in physiological condition. In conclusion, these biodegradable Mg material presents a new paradigm in the field of biodegradable medical devices.

1.2 The advantages of Mg as a biodegradable implant

Proper mechanical properties of biodegradable Mg

Magnesium is known to have suitable mechanical properties for orthopedic application, compared to traditional metallic implants or biodegradable polymer materials. Generally, the strength of Mg is higher than that of human cortical bone while Young's modulus (41-45 GPa) and density (1.74-1.84 g/cm^3) of Mg is close to those of bone (15-25 GPa and 1.8-2.1 g/cm^3). As shown in Table 1.1, commercialized metallic implants have considerably high Young's modulus, which can induce load concentration on the implant, causing stress shielding effect and attenuate density of the bone [8, 9]. However, similarity of Young's modulus of Mg and bone can alleviate re-fracture, which may be induced by the stress shielding effect during load transfer at the interface between implant and existing bone [3]. Mg-based materials are also known to have higher fracture toughness than bioceramic materials used for biomaterials and their compressive yield strength is similar to that of human cortical bone [8]. In addition, Mg has high thermal conductivity and excellent machinability, which makes it possible to fabricate individually patient-specific implants. These properties overcome the shortcomings of the conventional permanent metallic or polymeric materials and indicate that Mg and its alloy are more adequate candidates for practical biomedical applications [10].

Excellent biocompatibility and safety of biodegradable Mg

Magnesium is the fourth most abundant component in the human body and an essential element for numerous biochemical reactions and construction of bone and soft tissue. For regular functions, a healthy adult has to restore 24-30 g of Mg in the body and 310-420 mg of Mg is required daily to maintain health. Excessive Mg ions are released out of the body via the circulatory system or excreted through urine or faces, without any special side effects [11, 12]. Rather, Mg ions are known to promote bone regeneration and formation of new blood vessels, which demonstrates Mg ions can play a crucial role for treatment of bone disorders [13, 14]. Yoshizawa et al. reported that an addition of 10×10^{-3} M Mg ions augmented ECM mineralization by promoting several beneficial factors, such as collagen-X and vascular endothelial growth factor (VEGF) [15]. Furthermore, Mg ions at same dose induced activation of integrin and focal adhesion of human bone marrow mesenchymal stem cells (hBMSCs), which plays an important role in osteogenesis [16]. An *in vivo* results performed by Witte et al. suggested osteoblastic response and bone mass were improved around Mg alloys implanted into the guinea pig femur [17]. Moreover, main by-products of Mg-based materials generated under physiological condition, such as $Mg(OH)_2$, $MgCO_3$, $Mg_3(PO_4)_2$, $CaCO_3$ and $Ca_3(PO_4)_2$, are

phagocytosed by macrophage, which implies by-products are not detrimental to human body. [18]. All the more, degradation products can stimulate and accelerate bone growth, regeneration because formation of biological apatite, such as hydroxyapatite (HA), can be promoted [8]. In conclusion, Mg and its alloys have excellent biocompatibility and safety and their by-products generated during the corrosion process are not harmful to the human body, but rather, they are excellent materials that help bone formation and regeneration.

1.3 The limitation of biodegradable Mg implants

Despite many advantages, the practical use of Mg-based implants has been restricted because of high corrosion rate under physiological condition. As the body fluid is an aqueous solution containing many kinds of soluble ions, the Mg surface rapidly reacts with aqueous solutions. In particular, chlorine ions in body fluid are known for main component, accelerating the degradation of Mg [19-21]. The following equations are formula of corrosion reactions on pure Mg [22]:

$Mg \rightarrow Mg^{2+} + 2e^-$ (anodic reaction)

$2H_2O + 2e^- \rightarrow H_2 + 2OH^-$ (cathodic reaction)

$Mg^{2+} + 2OH^- \rightarrow Mg(OH)_2$ (product formation)

$Mg(OH)_2 + 2Cl^- \rightarrow MgCl_2 + 2OH^-$ (product dissolution)

The above reactions take place at the entire surface of magnesium where galvanic coupling generates due to potential difference between Mg matrix and intermetallic phase or grain boundary [23]. Magnesium hydroxide ($Mg(OH)_2$) is accumulated on the surface of Mg as a protective layer in wet condition. However, the body fluid contains chloride of about 150 mmol/L, which leads to vulnerable to $Mg(OH)_2$ layer. In general, $Mg(OH)_2$ begins to be converted to magnesium chloride ($MgCl_2$), which is soluble in water, in a solution containing more than 30 mmol/L of chloride [24]. Therefore, chloride starts to impair the $Mg(OH)_2$ protective layer, which results in pitting corrosion on the Mg surface. Eventually, accelerated corrosion rate of Mg induces degeneration of the mechanical strength and the failure of the material before the regeneration of surrounding tissue is completed [25]. In addition, hydroxide ions and hydrogen gas are generated as a by-product during corrosion. These by-products are rapidly generated and accumulated in the body, which incurs detrimental effects. Alkalization by released hydroxyl ions (OH^-) in the surrounding tissues hinders tissue regeneration, and in severe cases, causing chronic inflammation and necrosis of surrounding tissue. In addition, rapidly

accumulated hydrogen gas in the tissues can delay regeneration and induce tissue necrosis, forming a gas pocket between tissue and tissue's layer [26-28]. For these reasons, controlling the degradation/corrosion rate of Mg is considered to be important issue for practical use.

Firstly, there is the approach to control the composition and microstructure, including the grain size or texture of Mg itself, through alloying and optimizing manufacturing conditions. In particular, alloying with a relative noble metallic component is regarded as effective approach to control corrosion rate of Mg. Representatively, Aluminum (Al), Zinc (Zn), manganese (Mn), calcium (Ca) have been used to make less corrosive Mg alloy while controlling their contents or plastic deformation, heat treatment [29-31]. However, most studies of the Mg alloys are designed for industrial application with potentially toxic elements, which implies these toxic materials can induce unexpected clinical issues.

Secondly, surface treatment or coatings are considered as attractive way to control corrosion rate of Mg and improve biocompatibility via forming additional coating layer on magnesium surface, such as bioceramic or bio-polymeric layer. Surface coatings make inherent properties of Mg maintain, while imparting desirable functions for biomedical applications.

1.4 Surface coating on Mg to control corrosion rate

Surface coating has been investigated as one of the most studied and used strategies for practical use of Mg-based devices through fabricating additional layer without impairing the intrinsic properties of Mg while it presents better performance in reducing corrosion rate and improving bioactivity. The coating layer on the Mg surface generated by a variety of methods can block direct contact with water or other electrolyte ions contained in the physiological environment and serve as a physical protective layer. As a result, surface coating would minimize hydrogen gas evolution or excessive hydroxyl ions, which could be detrimental to tissue regeneration, and alleviate adverse effects. Additionally, biological performance, such as biocompatibility or hemocompatibility, can be greatly improved, depending on coating materials. There are various coating techniques and material depending on their applications. Typically, anodization, micro-arc oxidation, ion implantation, chemical conversion coating, electrodeposition, alkali heat treatment and sol-gel methods are used for surface coating. Moreover, according to coating material, it is categorized into a calcium phosphate-based bioceramic coating and a bio-polymeric coating [32].

1.4.1 Bio-ceramic surface coating

Bio-ceramic surface coatings have many attractive advantage for biomedical applications because they show excellent corrosion resistance or wear resistance and biocompatibility. In particular, calcium phosphate based coatings have similar composition and structure to those of natural bone, which leads to suppressing immune response and improving biological properties with osseous tissues [33, 34]. Representatively, hydroxyapatite (HA), dicalcium phosphate dihydrate (DCPD), tricalcium phosphate (TCP) and aluminum calcium phosphate (ACP) have been extensively used for biomedical fields since these ceramics show rapid integration with human body, outstanding osteoconductivity and osteoinductivity [21]. Consequently, there is a lot of interest and attractive in calcium phosphate based ceramic coatings on magnesium-based biomaterials [35, 36].

Various technique about calcium phosphate coatings have been conducted in previous research, showing outstanding performance for enhancing corrosion resistance. Hiromoto et al. suggested a high-crystalline HA coating layer on pure magnesium using a one-step hydrothermal method based on Ca-EDTA ($C_{10}H_{12}N_2O_8Na_2Ca$) solution. The formed HA coating layer with high crystallinity presented a lower solubility than the amorphous HA layer, which resulted in excellent stability. Owing to HA coating, the corrosion rate of Mg

was reduced, significantly [37]. Yang et al. introduced another HA coating method by immersing Mg into a calcification solution containing $Ca(NO)_3$, NaH_2PO_4 and $NaHCO_3$, at 37℃ for 48 h, followed by heat treatment of 2 h at 300℃. It was shown that the corrosion resistance of magnesium was also greatly improved due to the HA coating layer [38]. Zhang et al. also investigated biomimetical calcium phosphate coating method on pure Mg to improve corrosion resistance by immersing Mg substrate into simulated body fluid (SBF) for 24 h. They compared corrosion resistance single-coated (coating once) and dual-coated (coating twice) Mg sample with untreated Mg. They found corrosion protection was significantly improved in calcium phosphate coated Mg sample, compared to untreated Mg [34].

In addition to these bio-mimicking techniques, many studies have been also performed on the electrochemical deposition method. Song et al. reported hydroxyapatite was successfully coated on AZ91D alloy using electrodeposition method. By using electrolyte solutions containing $Ca(NO_3)_2$, $NH_4H_2PO_4$ and H_2O_2, hydroxyapatite coating was formed under a stable cathodic potential of 4 V for 2 h, followed by alkali treatment with 1M NaOH solution for 2 h. They proved hydroxyapatite coating fabricated by electrodeposition also showed much better corrosion resistance than that of uncoated Mg [39].

Fluoride treatment is also effective method for increasing corrosion resistance of Mg by forming magnesium fluoride (MgF_2). Typically, the coating procedure for fluoride treatment is conducted by immersion of Mg into hydrofluoric acid and MgF_2 was formed rapidly on the Mg surface. Chiu et al. obtained uniform MgF_2 dense coating of 1 μm thickness on pure Mg by immersing in hydrofluoric acid of 48 wt % for 6 and 24 h. The phase of coating layer contained amorphous phase, tetragonal MgF_2 and some $Mg(OH)_2$. They found that the corrosion resistance of MgF_2-coated Mg was greatly higher than untreated Mg in Hank's solution. The results indicate fluoride coating is a simple and promising method for enhancing corrosion resistance of Mg [40]. In addition, in the study of Witte et al, the LAE442 alloy was treated with 40 wt % hydrofluoric acid to form a MgF_2 layer on the surface. It was confirmed that the volume reduction of fluoride treated Mg samples was inhibited compared to untreated Mg through CT analysis, which demonstrated corrosion resistance was greatly improved by fabricating MgF_2 layer on the surface of Mg. Moreover, in the *in vivo* experiment, the immune response was also reduced on the MgF_2-coated Mg, relative to the sample without the MgF_2 layer [41].

Micro-arc oxidation (MAO) has also been considered an effective way for achieving protective uniform coating on the magnesium surface. MAO is a

method in which an electrochemical oxidation process is conducted on a magnesium surface with high voltage sparking in an electrolyte solution containing calcium and phosphate ions. Srinivasan et al. performed MAO technique using electrolyte solution containing $Ca(OH)_2$ and Na_3PO_4 with three mass ratio (1:2.5, 1:5 and 1:7.5) on AM50 alloy. On the AM50 surface, a coating layer composed of MgO and $Mg_3(PO_4)_2$ was formed, and the composition was shown to vary depending on the concentration and conductivity of the phosphate ion dissolved in the electrolyte. Among several ratios, the coatings obtained from the 1:5 ratio electrolyte showed an outstanding corrosion resistance, which is contributed to thickness, compactness and chemical composition of this coating [42].

1.4.2 Bio-polymer surface coating

Polymeric surface coating has been considered as another promising candidate for coating material to control corrosion rate of Mg implant. Polymeric materials have been already studied and used in a variety of biomedical applications, such as drug carrier, contact lenses, catheter, membranes because they have various chemical and physical properties [43]. Based on intrinsic properties of polymeric material, polymer coatings have been extensively focused as an available approach to control biological

response, such as cell adhesion, proliferation and differentiation since they have proper biocompatibility and bioactivity [44]. Representative polymer coating materials include synthetic polymers, such as Polycaprolactone (PCL), poly (L-lactic) acid (PLLA), poly (DL-lactide-co-glycolide) (PLGA) and polydopamine (PDA), and natural polymer, such as chitosan or collagen [25]. These various polymer coatings serve to improve the corrosion resistance of Mg, leading to reduce the initial corrosion rate under physiological condition and to be gradually degraded over time [23]. In conclusion, Mg and Mg alloys applied polymeric coating have been regarded as a prospective option because of their corrosion resistance, biocompatibility, self-healing, drug or biomolecule delivery and osteoinduction [25].

Li et al, reported PLGA coating on Mg6Zn alloy improved corrosion resistance, significantly. The coating thickness was about 33 and 72 μm, determined by concentration of PLGA solution. The corrosion rate of PLGA coated Mg alloy was reduced in NaCl solution, compared to uncoated Mg alloy. Also, the thicker PLGA coating showed better corrosion resistance than that of the thinner PLGA coating. They confirmed that, in *in vitro* cell test with MC3T3-E1 cells, the attachment of cells on the thin PLGA coated Mg alloy was exhibited better than uncoated Mg due to the PLGA coating [45].

Chen et al. conducted PLGA coating, which was capable of carrying a drug

while improving corrosion resistance of Mg alloy. After the inhibitor called benzotriazole (BTA) was dissolved in the PLGA solution, the PLGA coating layer was formed on the Mg alloy using an electrospray method, which could enhance corrosion resistance of Mg alloy. In addition, the PLGA coating layer was influenced by the surrounding pH and water, accelerating the release of BTA to obtain a protective effect by suppressing additional corrosion [46].

Furthermore, Wong et al. suggested that air-sprayed coating method with PCL in dichloromethane (DCM) on AZ91 alloy and porous PCL coating was obtained. They indicated the corrosion rate of the PCL coated Mg alloy was reduced and mechanical properties was maintained after degradation. In *in vitro* cytocompatibility tests with eGFP and SaOS-2 osteoblasts, better biocompatibility was identified on the PCL-coated Mg. Moreover, the in vivo study exhibited that the corrosion rate of uncoated Mg was much higher than that of PCL coated Mg and new bone formation around PCL coated Mg was better than uncoated Mg without any inflammation, necrosis or hydrogen gas pocket [47].

Mushahary et al. evaluated the corrosion resistance and the degree of bone mineralization by coating Collagen type-I (Coll-I), which is known for typical natural polymer, on Mg-Zr-Ca alloy. It was confirmed that an excellent trabecular bone structure around the Coll-I coated Mg specimen was observed

due to improved hydrophilicity of the surface, while showing better osteoinductivity and stabilization. In addition, they found that initial attachment of osteoblast cell was affected, depending on the monomer, of Coll-I, concentration, pH, surface roughness [48].

Various surface coating techniques and materials have been introduced to improve corrosion resistance and biocompatibility of Mg and Mg alloys. However, more researches have to be required for practical biomedical application, such as dental, orthopedic and vascular stent because any surface coating did not clearly resolve the clinical concerns or issues depending on the medical situation or patient's condition. Therefore, additional advances and innovations in durability, integrity and safety of the coating layer should be essential for commercial utilization of Mg implants.

Materials	Density (g/cm^3)	Elastic modulus (GPa)	Tensile strength (MPa)	Compressive strength (MPa)
Cortical Bone	1.8-2.1	15-25	110-130	100-230
Magnesium	1.74-2.0	41-45	90-190	100-140
Ti alloy	4.4-4.5	105-113	900-950	896-1172
Co-Cr alloy	7.8	195-230	450-960	450-1000
Stainless steel	7.9	200	490	480-620

Table 1.1 Mechanical properties of various metallic implant materials in comparison with cortical bone (Redrawn from ref [3, 49]).

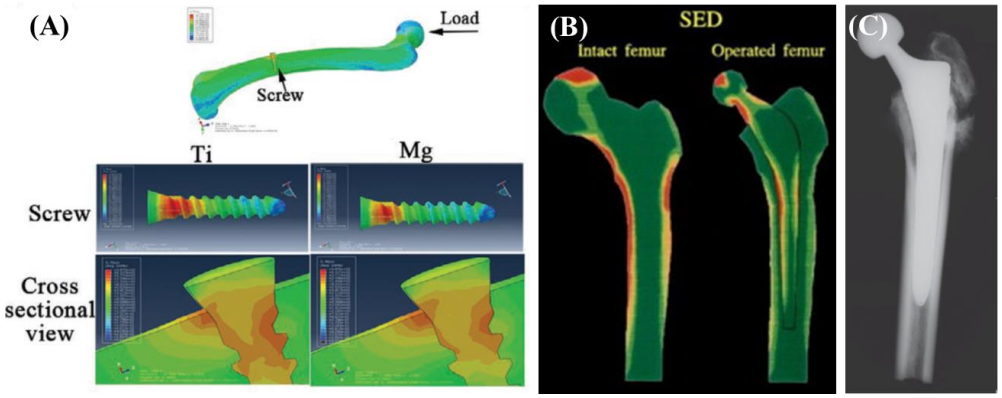

Figure 1.1 (A) The peak stress distribution applied in an implanted Ti and Mg-based screw in a femur using a finite element analysis (FEA) and (B) illustration of stress energy density before and after implantation and (C) clinical X-ray radiograph of a human femur with artificial hip-joint implantation (Redrawn from ref [12, 50, 51]).

Chapter 2.

HA-PEI hybrid coating on groove pattern for biodegradable Mg orthopedic implants

2.1 Introduction

Functional coating is a promising approach to adjust the surface characteristics of a material. Functional coatings is known to improve mechanical protection, chemical resistance, biological performance, and response to external stimuli [52-57]. However, under external deformation, the coating layers on deformable substrate can cause mechanical defects such as buckling, cracking, and delamination at the interface because the large deformation discrepancy is induced due to different materialities between the two materials under an external force [58-61]. For example, flexible electronic devices are inclined to generate defects, such as wrinkling, cracks, and interfacial delamination of the thin metallic or composite films under compression, tension, or bending [59, 60]. As a result, new coating strategies that augment the mechanical stability of coating layer under various situations have been desired [58, 62]. In previous researches, applied stress and strain was gradually distributed by arranging graded layer between coating and substrate, which could suppress delamination caused at the interface [63]. As other methods, the contact stability could be enhanced with a new flexible coating materials that better fit the base material or by buckling-induced metallic films on a pre-deformed substrate for a stretchable metal wires [64, 65]. However, in spite of these advantages, the thickness of coating layer could be limited and

the fatigue in coating layer may suppress the long-term stability for practical application [66]. The coating-substrate interface problem also has been emerged in coating layer on magnesium (Mg)-based implants.

Magnesium (Mg) and its alloys have been widely investigated for orthopedic biomedical applications due to good biocompatibility, biodegradability and suitable mechanical properties [36, 67, 68]. Mg-based implants can be degraded in human body without toxicity and Mg ions released from Mg implants are known to be beneficial to cellular response, angiogenesis and tissue regeneration [36, 69, 70]. In addition, its mechanical properties are similar to natural cortical bones, which can prevent 'stress shielding effect'. Moreover, biodegradability can eliminate the need for a secondary surgery, which alleviate patient's additional pain, cost and surgical procedure [36, 68]. However, despite these superior advantages of Mg-based implants, practical use of Mg in biomedical applications is difficult because of its fast corrosion rate in physiological environment. During corrosion process in physiological condition, evolved and accumulated hydrogen gas can form gas pocket and interfere with cell adhesion on the implant surface. Also, alkalization induced by released hydroxyl ions damages tissues around the implant and leads to necrosis of tissue. Besides, mechanical properties of Mg-based implants deteriorate rapidly, which could cause failure of Mg-based implants before

completion of tissue regeneration [36, 67-71].

Many studies, such as alloying [17, 72-74] and surface treatment [39, 75, 76], have been investigated to improve corrosion resistance of Mg-based implants. In particular, surface coatings on Mg is classified to polymer coating and ceramic coating. Polymer coatings, such as Poly l-Lactic acid (PLLA) [77] or Polycaprolactone (PCL) [78, 79], show resistance to deformation because of their flexibility. Among several biopolymers, polyetherimide (PEI) is known to have good corrosion resistance and adhesion strength to Mg but it has inferior biocompatibility to bioceramic [80]. On the other hand, calcium (Ca) and phosphate (P) based bioceramic coatings have been studied in many literatures since these coatings not only enhance corrosion resistance but also improve biocompatibility. Most calcium phosphate compounds, such as Hydroxyapatite (HA), Tri-calcium phosphate (TCP) and Di-calcium phosphate dehydrate (DCPD), have excellent biocompatibility and bioactivity into the bone cells, which result in better osteoconductivity because their components are similar to the human bone [81]. However, these ceramic coatings can lead to cracks and delamination when deformation is applied to Mg implant because of their brittleness [82, 83]. In practical medical situation, the coating materials on Mg-based implants must be mechanically stable even under deformation during surgical operations. In addition to the load-bearing role of the implant, the

substrate will be deformed post-surgery by bone regenerated through the healing process [84-86]. As a result, the surface of Mg is exposed due to inevitable deformation and contacts with water and electrolyte in body fluid, accelerating corrosion of Mg. Undesirable corrosion of Mg can incur mechanically failure of Mg-based implant and unexpected adverse effect to tissue regeneration.

In order to solve the problem, our study focuses on applied strain distribution at the interface between the substrate and the coating layer. On the flat surface, applied strain at the whole interface can result in defects in the coating layer under deformation. Thus, strain distribution applied at the interface is required to be controlled for restriction of defect formation. Several studies have already proved that strain distribution caused on the surface could be controlled depending on surface morphology under deformation [87]. In particular, on the surface which has a variety of wrinkle patterns, strain is concentrated on the inner part of wrinkle patterns under deformation.

In this study, we developed ceramic-polymer hybrid coating selectively by introducing groove patterns. Firstly, groove patterns on the Mg surface were designed using finite element analysis (FEA), which can concentrate strain at inner part of groove. Then, HA was coated on the hill part of groove pattern where strain was applied relative minimally and PEI was

coated in the valley part of groove pattern because applied strain was concentrated in valley part. By regulating strain distribution, crack formation and propagation were prevented and morphology of coating layer was maintained after tensile deformation. Moreover, corrosion resistance of the hybrid coating layer was characterized with variation of pH and released hydrogen gas during corrosion in SBF. Furthermore, in order to evaluate biological performance, morphologies of pre-osteoblast cells attached on the coating surfaces were observed with SEM.

2.2 Material and methods

2.2.1 Computational modeling with finite element analysis (FEA) models

In order to optimize scale of groove patterns, finite element method (FEM) simulation was conducted using Abaqus/CAE/standard 6.13 (Simulia, Dassault Systemes, Providence, RI, USA). The micropatterned Mg was designed Mg substrate (thickness: 10 mm) with or without HA-PEI coating in FE models. In all FE models, the Mg surface was patterned with sinusoidal undulations using a fixed wavelength (λ=50 μm) and various amplitudes (A=0–50 μm), ensuring that A/λ was within a range of 0–1. In experimental measurements of HA-PEI coated Mg, the HA and PEI layers were maximally thick (8 μm and 4 μm, respectively) at the peaks and valleys of the Mg substrate, respectively. The material properties of Mg and PEI were determined by fitting the stress–strain curves obtained from tensile tests. Assuming J2 plasticity models, we obtained E=44.7 GPa, σ_y=44 MPa, and ν=0.29 for Mg and E=149.8 MPa, σ_y =16 MPa, and ν=0.4 for PEI. The E and ν values for HA were estimated at 60 GPa and 0.3, respectively [88]. The total area was calculated using the following equation: $\Gamma = \int_0^{\lambda} \sqrt{1 + \left(\frac{dy}{dx}\right)^2}\, dx$. In all FE simulations, we imposed periodic boundary conditions to represent an infinite number of representative units. All FEA models used plain strain elements (CPE4R in the ABAQUS element library). The appropriate mesh size for accurate computations was

determined from mesh-sensitivity studies.

2.2.2 Material preparation

Pure Mg samples with flat dog-bone shape were prepared from the commercial pure (99.99 wt%) Mg ingot (Yirium, China) with a gauge length, thickness and width of 10, 2, and 3 mm, respectively. The specimens were polished with SiC abrasive papers (up to 1200 grit), cleansed with ethanol in ultrasonic bath and dried in air. Microgroove patterns on Mg substrate was fabricated by laser machining procedure using ND:YV04 UV Laser system (AWAVE 355-10W-30K, Advanced Optowave, NY, USA). The wavelength of laser beam and marking power was 355 nm and 0.9 W, respectively, and the laser pulse frequency and duration was 30 kHz and 10 μs. Marking speed of laser machining was 500mm/s. The width, depth and spacing of the fabricated microgrooves are 20 μm, respectively. The experimental procedure of the HA-PEI coated Mg with micropattern was shown in **Figure 2.1**. Firstly, for the PEI (polyetherimide) coating, PEI pallet (Sigma-aldrich, USA) was dissolved in N-methyl-2-pyrollidone (NMP) with a concentration of 10% w/v and was stirred at 37℃ for 24 h. After the PEI solution was prepared, the PEI layer was spin-coated at a spin rate of 4000rpm for 1 min. The PEI coated Mg specimens were dried at 70℃ for 1 day to eliminate the residual solvent. Subsequently, HA was coated onto the PEI coated Mg sample by immersing in HA coating solution.

The treatment solution was based on the procedure reported by Kim et al [89]. The solution was prepared with 0.05 M ethylenediaminetetraacetic acid calcium disodium salt hydrate (Ca-EDTA)/0.05 M potassium dihydrogen phosphate (KH_2PO_4). The pH of the solution was adjusted to 8.9 with sodium hydroxide (NaOH). The PEI coated Mg specimens were immersed in the coating solution and reacted at this conditions for 2 h at 90℃. The coated Mg specimens were rinsed with distilled water and dried in air. To evaluate performance of the HA-PEI coating layer, a 5% tensile strain deformation was applied to the samples using Instron tensile machine (Instron 5582) at a rate of 0.5mm/min.

2.2.3 Material characterization

The surface morphologies of the samples were observed using scanning electron microscopy (SEM, JSM-6360; JEOL, Japan) and field-emission scanning electron microscopy (FE-SEM, JSM-6330F; JEOL, Japan). The cross-section of the samples was studied using FE-SEM and Focused Ion Beam (FIB, AURIGA, CarlZeiss, Germany). For observing cross-sectional views with SEM, the samples were mounted in epoxy resin for 1 day and were sectioned by a low speed saw (No.11-1280ISOMET, Buehler, USA). Then, the cross-sections were polished up to 0.04 μm silica suspension and cleaned with

ethanol. The crystalline structure of the HA-PEI coated Mg specimen was examined by X-ray diffraction at a scan speed of 5°/min (XRD, D8-Advance; Bruker, Germany) To evaluate mechanical stability of the HA-PEI coating layer, a 5% tensile strain was applied to the samples using Instron tensile machine (Instron 5582) at a rate of 0.5mm/min.

2.2.4 *In vitro* Corrosion behavior

The corrosion behavior of the samples before and after deformation was assessed with simulated body fluid (SBF). The Bare Mg, the HA coated Mg, the HA-PEI coated Mg with micropatterns before and after deformation were immersed in 40ml of SBF at 37℃ for 7 days, followed by pH variation of SBF and the amount of evolved hydrogen gas were monitored. The SBF was prepared using the method proposed by Kokubo et al [90]. The pH value was measured with pH meter (Orion 3 Star, Thermo Scientific, USA) and the volume of released hydrogen gas was collected and recorded. After corrosion for 7 days in SBF, the surface morphologies of the HA coated Mg and the HA-PEI coated Mg were confirmed with SEM.

2.2.5 *In vitro* biocompatibility test

For the in vitro cell tests, the samples (bare Mg, HA coated Mg, and

HA-PEI coated Mg) were cleaned using ethanol and sterilized by ultraviolet irradiation in a clean bench. Before *in vitro* test, pre-osteoblast cells (MC3T3-E1, ATCC, CRL-2593) were cultured in an alpha minimum essential medium (α-MEM, Welgene Biotech Co., Ltd., Gyoengsan, Korea) supplemented with 10% fetal bovine serum and 1% penicillin–streptomycin. The cells were seeded on the samples at density of 5×10^3 cells/ml and cultured for 5 days in humidified incubator under air atmosphere containing 5% CO_2 at 37℃. After culturing for 5 days, the attached cells on the samples were observed using SEM. Prior to the SEM observation, the cells on the samples were fixed with 2.5% glutaraldehyde for 10 min, dehydrated in graded ethanol (75%, 95% and 100% ethanol in sequence) for 5 min each, and immersed in hexamethyldisilazane for 10 min and dried in air.

2.3. Results and discussion

2.3.1 Determination of surface pattern through FE analysis

Strain contours on the Mg surface with the flat surface and wavy geometry was compared in FE model and under 3% global tensile strain (**Figure 2.2**). On the flat Mg substrate, the strain contour revealed uniform distribution in accordance with 3% global strain (**Figure 2.2A**). In contrast, the strain contours on the wavy patterned surface presented interesting features; strain in the hill parts was nearly zero while a localized strain of ~ 0.16 appeared in the valley part of the wavy surface (**Figure 2.2B**). The strain contours were exhibited similar under higher global strains (> 3%), which demonstrates that brittle and flexible coating materials can be introduced to regions with small and large deformations, respectively (**Figure 2.2B**). Before coating on the Mg surface with HA and PEI, we determined the appropriate one-dimensional (1D) patterns on Mg by simulating the FE models. Micro-pattern on the Mg surface was assumed with a 1D sinusoidal wavy shape described by $y = A \cdot \sin\frac{2\pi}{\lambda}x$, where A and λ denote the amplitude and wavelength of the pattern, respectively (**Figure 2.3A**). The hill parts of groove pattern were rarely deformed under tensile deformation, whereas the valley parts were locally deformed. Also, in order to determine the aspect ratio of groove patterns, we tried various aspect ratio of the patterns (where an aspect ratio of 0 denotes a flat surface), fixing

the tensile strain at 3%. Increasing the aspect ratio from 0 to 1 significantly increased the localized strain in the valley parts (ε_{val}) and the effective surface area (Γ/λ) associated with the area of HA coating, where Γ denotes the total surface area of the patterned Mg surface. For aspect ratios of A/λ exceeding 0.1, the strain induced in the hill parts (ε_{peak}) was < 0.1%. Also, according to our experimental results, failure of pure Mg occurred under strains of between 15% and 16%; therefore, to avoid fracture in the valley regions of the patterned Mg surfaces, we limited the aspect ratio (A/λ) of groove pattern to < 0.4. Applying different material to the Mg substrate, the coating layers might also endure the deformation of the patterned surfaces (**Figure 2.3B).** We applied the flexible PEI coating on the valley parts and brittle HA on the hill parts. The standard of critical global strain was determined by the following three criteria: 1) maximum local strain on the Mg substrate was below the strain at failure (16%), 2) maximum local strain on the PEI coating was below the strain at failure (20%), and 3) maximum local strain on the HA coating was below 0.1%. Meanwhile, the effective surface area should be maximized such that the HA coated surface area of the HA-PEI coating layer approximately equals or exceeds the flat Mg surface area. At an aspect ratio of 0.4 (A/λ =0.4), the critical global strain was between 3% and 4%, and the effective surface area was double that of the flat surface area (Γ/λ =1.9). Based on these results of FE models and resolution of laser machining, the wavelength (λ) and amplitude (A) was

determined to about 50μm and 20μm.

2.3.2 Characterization of the HA-PEI hybrid coating

Figure 2.4 shows surface morphologies of the bare Mg, the HA coated Mg and the HA-PEI coated Mg with micro-patterns. **Figure 2.4A** exhibits microgroove patterns of 20μm fabricated on Mg substrate by laser machining process and the groove patterns of curvy shape were shown uniformly well on the whole surface. **Figure 2.4B** shows morphology of the HA coated Mg with the micro-patterns. During HA coating procedure, HA was precipitated on the Mg surface by reacting with calcium ions and phosphate ions and formed as additional layer. In general, the characteristic structural feature of nano-crystalline HA is known to present the needle structure, which led to roughened surface. As a result, the HA coating layer was formed well regardless of complex structure of the micro-patterns. **Figure 2.4C** displays the surface morphology of the HA-PEI coated Mg with micro-patterns. HA was formed on only hill part and PEI was coated on valley part, selectively, as shown in **Figure 2.1**. In magnified image of the HA-PEI coated Mg, needle shape of precipitated HA crystal was shown clearly and smooth surface of PEI coating was observed on the valley part and interface between HA and PEI had discrete boundary.

Cross-sectional images of the HA-PEI coated Mg with micro-pattern

are shown in **Figure 2.5A**. HA coating layer on hill part was shown clearly with a thickness of 4-5μm and PEI coating of about 1-2μm layer was exhibited in valley part. Moreover, the measured HA coated surface area was almost one, suggesting that the surface areas of the HA coating layers were nearly equivalent on the patterned and flat Mg surfaces. In order to identify accurate mechanism of selective coating, magnified images of hill part was obtained using FIB, as shown in **Figure 2.5B**. On the hill part, any special interface or layer was not shown between HA and Mg substrate, which indicates HA and Mg were adhered to each other. In detail, from EDS result of **Figure 2.5B**, only calcium and magnesium elements were detected around interface between HA and Mg (red line) at the region, without any carbon layer. It indicates that HA was not formed on the PEI coating layer of hill part, and that the PEI coating layer was not involved in formation of HA coating layer on magnesium. Generally, if the spin coating is performed on the patterned surface using a polymer solution, the thickness of the coating layer is varied, depending on the roughness. In other words, a very thin coating layer is formed on the hill part of the groove pattern, and a relatively thick coating layer is formed on the valley part. Therefore, various ions in the HA coating solution permeated through thin PEI layer formed on hill part of groove pattern and react with the Mg substrate to precipitate HA. However, these ions are difficult to penetrate through thick PEI layer on valley part, which leads to selectively HA coating only on hill part

of groove pattern.

The XRD patterns of the HA coated Mg and the HA-PEI coated Mg with micro-pattern are exhibited, as shown in **Figure 2.6**. From the XRD patterns of the HA coated Mg (black line), representative peak of HA was shown at $2\theta = 26°$, which was similar pattern suggested by Kim et al [89], which ensure HA coating layer was obtained well, regardless of microgroove pattern. Likewise, at the XRD patterns of the HA-PEI coated Mg, representative peaks and intensities were same with those of the HA coated Mg. As mentioned in Figure 2.5, HA coating layer was formed well although PEI coating layer existed on the Mg substrate with micro-patterns.

2.3.3 Deformability of the HA-PEI hybrid coating

Mechanical deformability of the HA-PEI coated Mg specimen was examined under 5% tensile strain, compared with the HA-coated Mg with or without micro-patterns in **Figure 2.7**. According to the simulation results as indicated in **Figure 2.3B**, 5% deformation likely led to rupture of the patterned Mg substrate. The tensile tests with flat and patterned Mg substrates with the aspect ratio of 0.4 were conducted at different applied strains. In our experimental results, until 4% strain, all samples didn't show any crack, while at $\varepsilon \geq 5\%$, fractured Mg samples were found. In case of 5% strain, 1-2 samples

out of 10 were fractured, whereas 8% strain resulted in 100% failure of the whole specimen. Therefore, we chose 5% as the critical tensile strain for the further mechanical assessments. The discrepancy between the simulations and experiments may result from the variation of Mg samples (e.g., strain at failure of 15-20% [91, 92]) and structural disparity of created micropatterns on Mg. On the flat surface, 5% deformation occurred through the whole surface, thus the HA coating layer was cracked and delaminated since its strain at failure is less than 0.1% (**Figure 2.7A**). For the Mg surface with micro-patterns, 5% tensile strain induced different strain distribution with the flat surface, particularly, leading to the low strain level ($\varepsilon_{peak} < 0.1\%$) and the high strain level ($\varepsilon_{val} > 15$ %) on the hill and valley regions, respectively. In case of the single HA coating layer on the patterned surface as shown in **Figure 2.7B**, many cracks and delamination were observed on the HA coating layer. Cracks may be initiated at the valley regions under deformation and propagate along with the valley regions, normal to the loading direction. And then, these cracks led to additional propagation of cracks across the patterns, ending up with catastrophic failure throughout the Mg surface. However, on the HA-PEI coated Mg, any cracks or delamination was not found (**Figure 2.7C**). As assumption in this study, the applied strain to the flexible PEI layer was concentrated while the strain was hardly the strain applied to HA on the hill part. As a result, it was found that crack initiation did not occur anywhere, and the occurrence of

defects was significantly suppressed compared to the HA coated specimens, which demonstrates that the deformability of the HA-PEI coating layer was improved.

2.3.4 Corrosion behavior of the HA-PEI hybrid coating

The corrosion tests before and after deformation were performed in order to confirm the corrosion resistance of the coating layer for the underlying Mg substrate, regardless of deformation (**Figure 2.8**). To verify corrosion resistance of the HA-PEI coating layer, variation of pH and the amount of evolved hydrogen gas were monitored for 7 days after immersing in SBF. All Mg specimens were patterned to fix contact area with water for the corrosion tests. If a coating layer on Mg contains any potential defects, the corrosion rapidly occurs in chloride-containing water, indicating existence of surface crack or interfacial delamination which should cause direct exposure with aqueous solution. Without deformation, the HA or HA-PEI coated Mg specimens show significantly reduced corrosion rates under physiological conditions, compared to uncoated Mg as shown in **Figure 2.8A and C**. However, after 5% deformation, the generated cracks and delamination on the HA coated Mg resulted in creating direct contact paths of the underlying Mg substrate to water, increasing the corrosion rates (**Figure 2.8B and D**). On the

other hand, the HA-PEI coated Mg maintained good corrosion resistance regardless of deformation, featuring almost identical corrosion behavior before and after deformation. The surface morphologies of coated Mg specimens after corrosion for 7 days were observed as exhibited in **Figure 2.9**. Without deformation, the morphologies of the HA coated Mg and the HA-PEI coated Mg were sustained during corrosion test as shown in **Figure 2.9A and C** because these coating layer showed good corrosion resistance, as confirmed in **Figure 2.8A and C**. Under deformation, the applied strain was induced and highly localized at the valley region, which initiated surface cracks or delamination on the HA coating layer (**Figure 2.7B**). The surface cracks or detachment of fragments in the HA layer were acted as corrosion-initiation and reaction sites on the partially exposed Mg surface. Therefore, rapid corrosion occurred at the expose site and HA coating layer appeared to be damaged and lifted out by evolved hydrogen gas during corrosion, as shown in **Figure 2.9B**. By contrast, the almost crack-free HA-PEI coated Mg clearly maintained its morphology after corrosion test, exhibiting low corrosion rates over the immersion time (**Figure 2.9D**). As displayed in Figure 2.7C, on the surface of the HA-PEI coated Mg, any defects were not found even under deformation, which indicated corrosion-initiation sites were significantly restricted because exposure of Mg surface was minimized after deformation.

2.3.5 In vitro biocompatibility of the HA-PEI hybrid coating

In vitro cell attachment test was conducted using pre-osteoblast cells (MC3TC-E1) with the HA coated Mg and the HA-PEI coated Mg. **Figure 2.10** shows images of the attached pre-osteoblast cells on the surface of the samples without and with deformation after culturing for 5 days. On the surface of the HA coated Mg sample, pre-osteoblast cells were spread well on the HA coating layer as shown in **Figure 2.10A**. By contrast, on the surface of the HA coated Mg with deformation, the number of attached cells was reduced than that in the case of the HA coated Mg without strain and morphologies of attached cells was more spherical shape as shown **Figure 2.10B**, which resulted from fast corrosion caused from exposed Mg surface on the HA coated Mg under deformation. However, as displayed in **Figure 2.10C and D**, the pre-osteoblast cells on the HA-PEI coated Mg samples exhibited similar morphologies and numbers to each samples, regardless of deformation. Also, cells adhered on the HA-PEI coating layer were stretched along with direction of groove patterns, featuring that attached cells appeared to a longish and narrow shape. The attached cells on the HA coated Mg without deformation were attached well on the surface, which resulted from outstanding biocompatibility of HA coating [41]. However, after deformation, partial exposure of Mg surface was caused

by defects at the HA coating layer, which influenced cellular response as shown in **Figure 2.10B** due to the increased pH value and released hydrogen gas [93]. Generally, evolved hydrogen gas could interfere initial attachment of cells on the surface and alkalization also could disrupt attachment and proliferation of the cells [89]. In contrary to the HA coated Mg, corrosion resistance of the HA-PEI coated Mg was maintained regardless of deformation, which indicates that cell attachment was facilitated in favorable environment. In addition to corrosion effects on cell viability, surface patterns significantly affected cell morphology, alignment, and distribution on the Mg surface. Because topography of surface was influenced by coating layer, HA and HA-PEI coated surfaces showed different cellular responses. In the case of HA-coated Mg, HA coating was uniformly covered on the Mg surface with a thickness of 4-5μm. However, the HA-PEI coated layer had various local thicknesses depending on the region, with hill (4-5μm) and valley regions (1-2μm). As a result, the distance between hill parts in the HA-PEI coated patterns became wider than that in HA-coated patterns. This topographic difference influenced morphology and distribution of the adhered cells (**Figure 2.10**). Cells on HA coated Mg gathered on the hill regions instead of adhering in the valleys of the groove patterns. migrating from hill to hill part in a direction perpendicular to the groove patterns while being spread out on adjacent hill parts of groove patterns. By contrast, most cells appeared to attached in the valley parts of the HA-PEI

coated patterns, indicating that those patterns allowed cells to cover the entire surface of the groove pattern (**Figure 2.10C and D**). Interestingly, cells at the valley regions presented highly elongated morphologies with strong alignments parallel to the groove pattern direction, following this cellular response referred to as "contact guidance effect" [94, 95]. Previous studies have reported that cells adhere to the surface with alignment along the pattern direction when the pattern wavelength is comparable to the size of the spread cells [96-98]. In this work, wavy HA-PEI coated patterns could provide strong cell alignment in one direction as compared with HA coated patterns, even though both coatings had the same wavelength of groove pattern (~50 μm). The strong alignment of cells on the HA-PEI coated patterns can likely be attributed to the wider distance and higher height of the patterns [96, 98]. The cells localized within the deep valley parts might spread out along the groove pattern direction instead of moving to adjacent patterns. As a result, the HA-PEI coated Mg could induce elongated morphology of cells, which is able to promote differentiation of osteoblast compared to flat surface as reported in many literatures [99]. Thus, the HA-PEI coated Mg with micro-patterns was expected to enhance cell proliferation or differentiation by inducing alignment or orientation along with groove structure.

2.4 Conclusion

In summary, we presented a novel approach for a robust rigid coating method on a deformable substrate, by incorporating the structural modification of the substrate surface for deformation gradient. As a proof-of-concept, a corrosion resistant coating layer on Mg consisting of both polymeric and ceramic materials was developed using both computational and experimental methods. The computational simulations with micropatterned Mg provided the design guideline of the patterns in order to avoid any failure due to localized strain associated with pattern geometry. The uniform groove pattern with micro-scale was fabricated with laser machining. And then, the HA-PEI selective coating was achieved by spin-coating and hydrothermal procedure. The HA-PEI coated Mg surface clearly exhibited good mechanical stability, corrosion resistance and biocompatibility regardless of applied deformation, with the maximized surface area of bioactive HA coating regions. Therefore, we proved that a rigid coating layer can be incorporated into a deformable and stretchable substrate without failure by controlling surface geometry of the underlying deformable substrate.

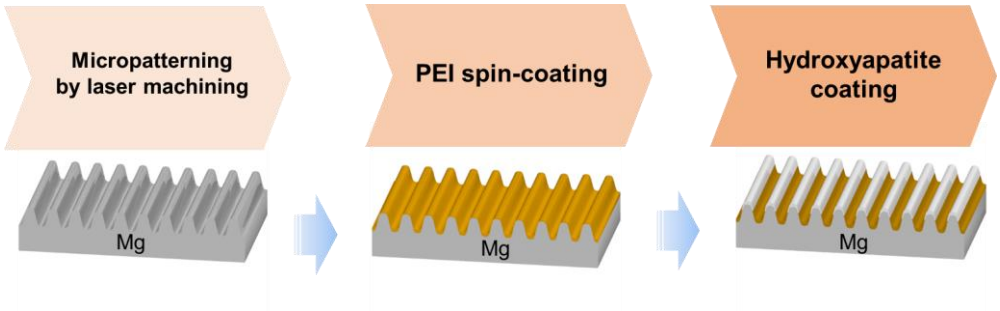

Figure 2.1 Experimental procedure of the HA-PEI coated Mg with micropatterns.

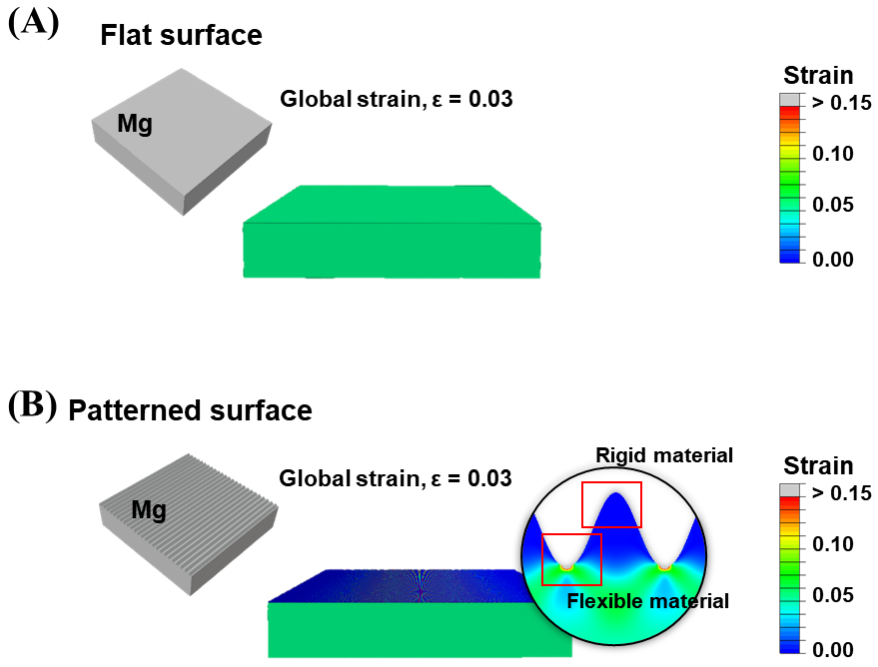

Figure 2.2 Strain contours (A) on the flat and (B) micropatterned Mg samples under an applied global strain of 3%.

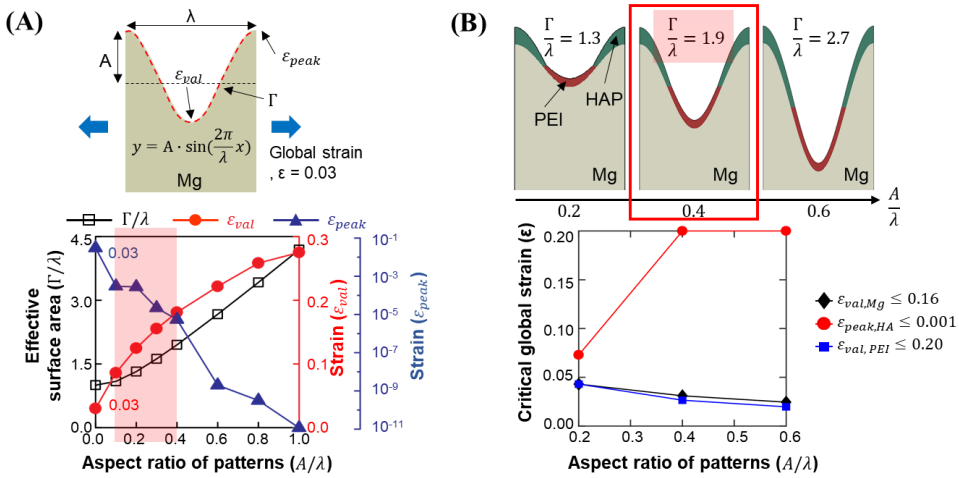

Figure 2.3 Computational design of the micropatterned Mg surface. (A) Effective surface area of the sinusoidal micropatterns under a 3% strain (applied at the valley). (B) Critical global strain on the PEI/HA-coated micropatterned Mg surface under a 3% applied strain. The equalities indicate the strain at failure of Mg, PEI, and HA.

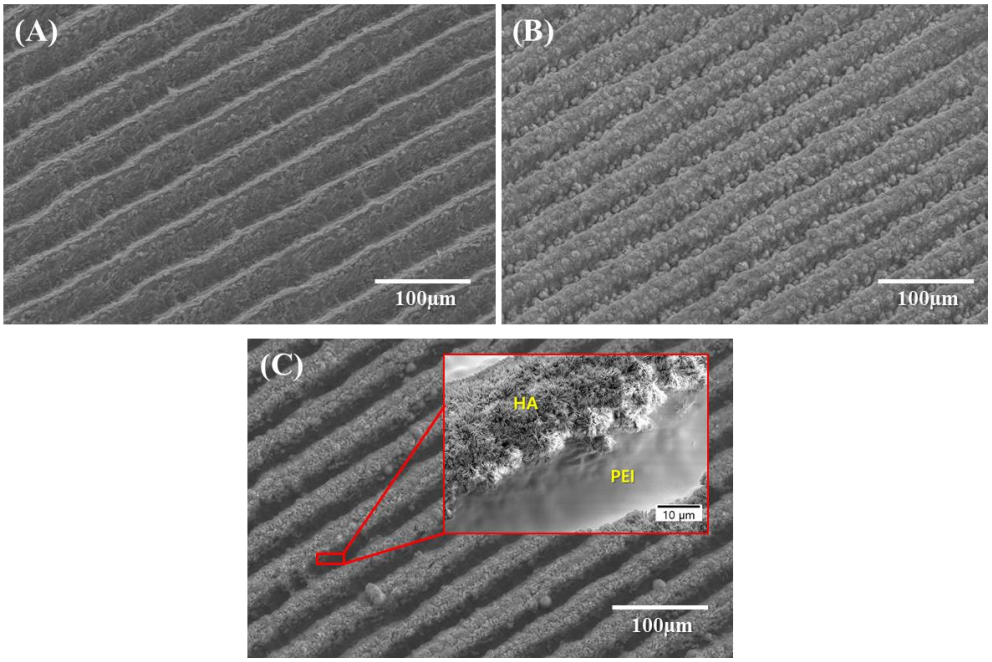

Figure 2.4 Surface morphologies of (A) the bare Mg, (B) the HA coated Mg and (C) the HA-PEI coated Mg with micropatterns.

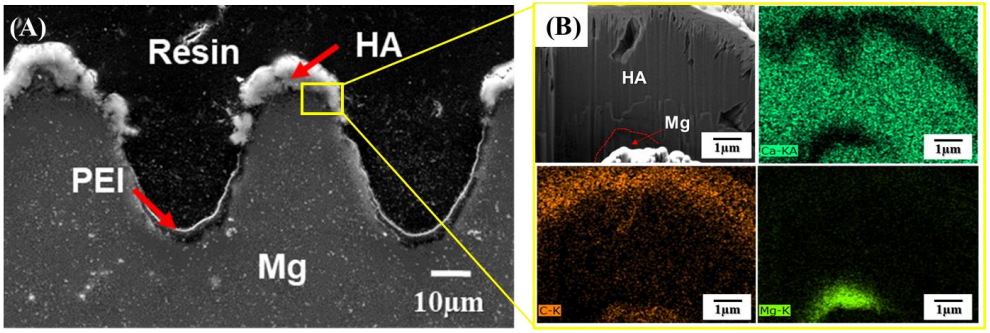

Figure 2.5 (A) Cross-sectional SEM images and (B) EDS mapping of the HA-PEI coated Mg with micropatterns.

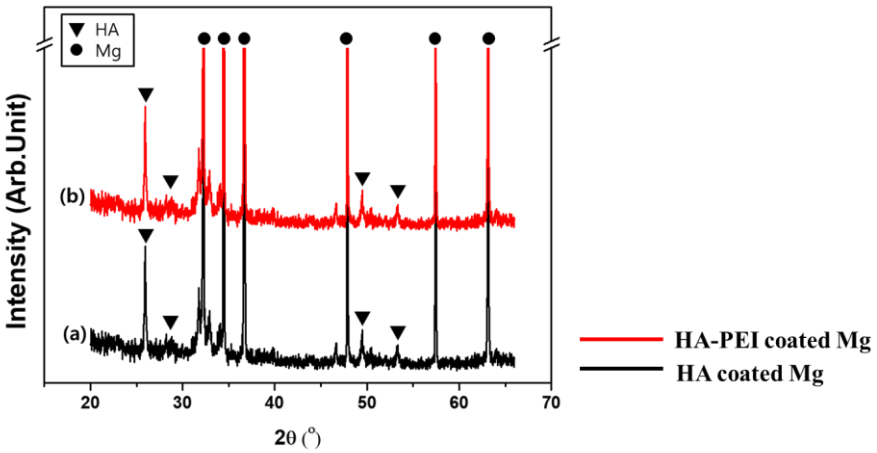

Figure 2.6 XRD patterns of the HA coated Mg (black) and the HA-PEI coated Mg (red) with micropatterns

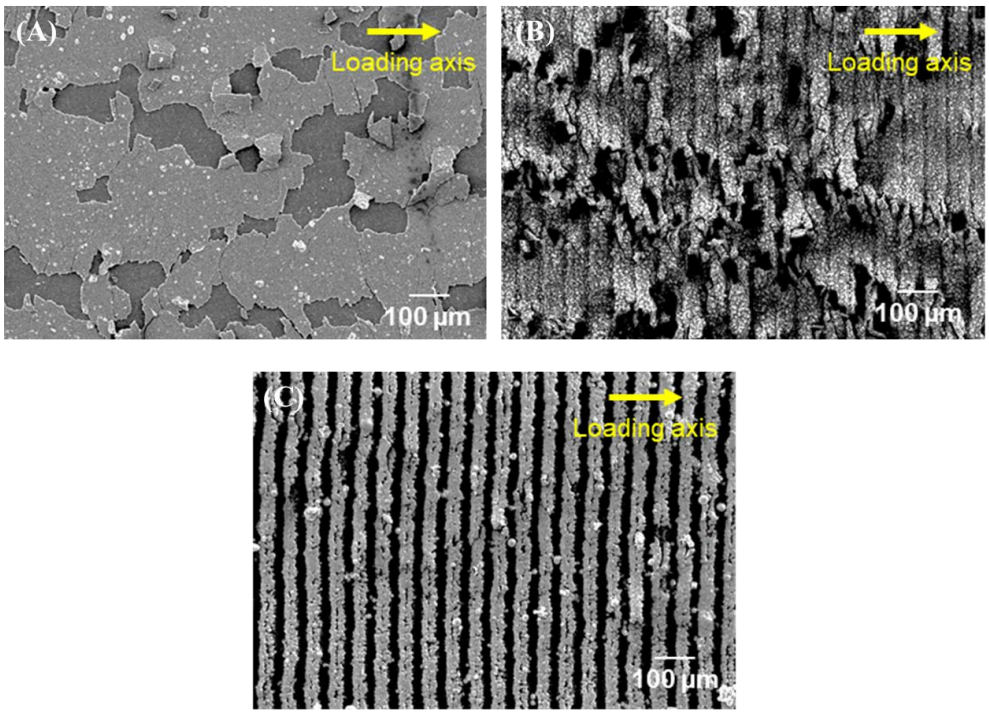

Figure 2.7 Surface morphologies of the HA and the HA-PEI coated Mg after 5% deformation. (A) HA coated Mg with flat surface, (B) HA coated Mg with micropatterns, and (C) HA-PEI coated Mg with micropatterns.

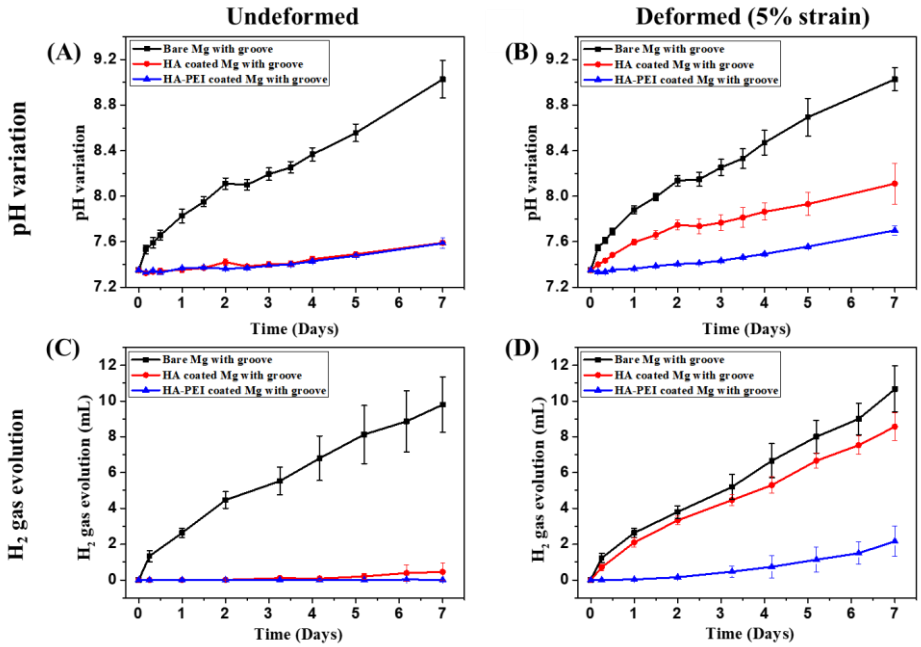

Figure 2.8 Corrosion behaviors of the bare, the HA and the HA-PEI coated Mg samples with micropattern after immersion for 7 days in SBF at 37 °C. pH values of the samples throughout the 7-day immersion (A) before deformation and (B) after 5% deformation of the samples. Evolved H_2 gas of the samples throughout the 7-day immersion (C) before deformation and (D) after 5% deformation of the samples.

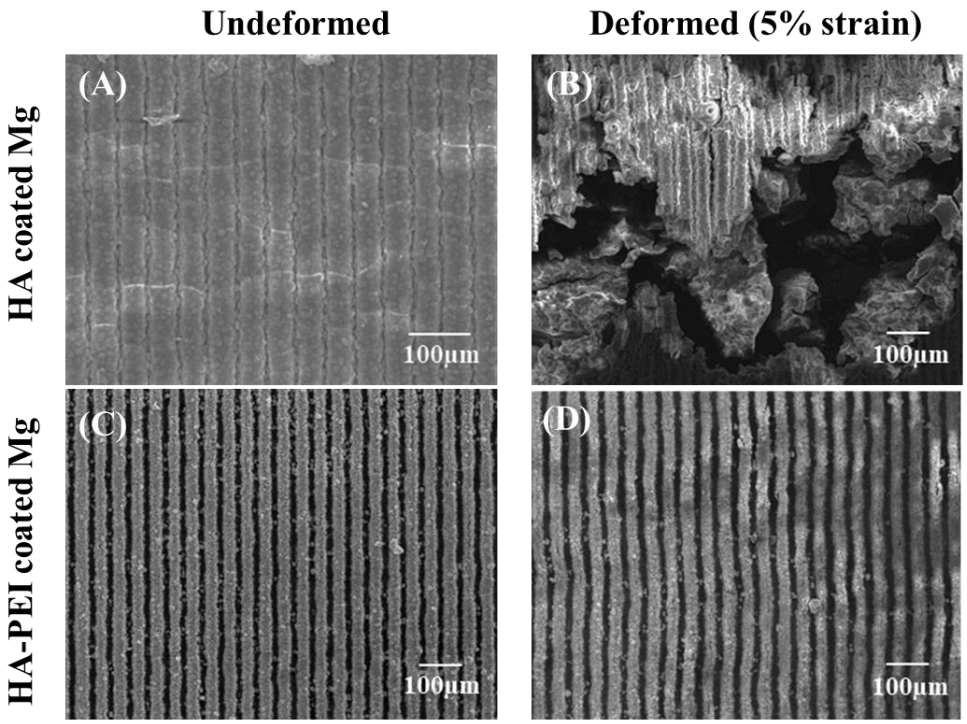

Figure 2.9 Surface morphologies of the HA and the HA-PEI coated Mg after immersion for 7 days: HA coated Mg samples (A) before deformation and (B) after deformation. HA-PEI coated Mg samples (C) before deformation and (D) after deformation.

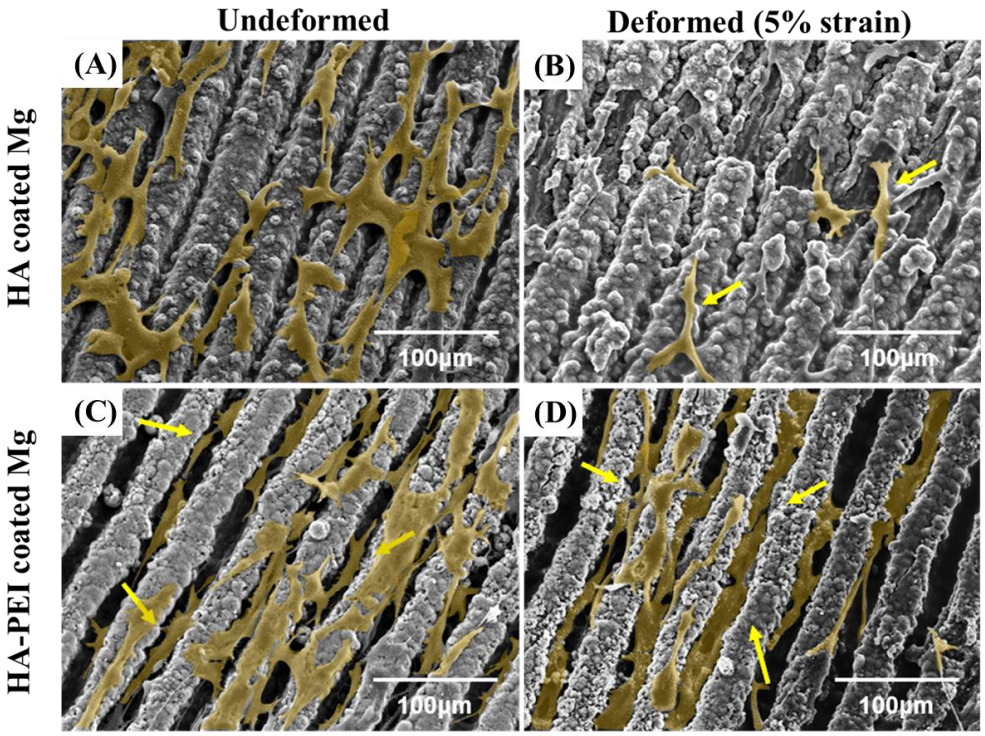

Figure 2.10 Cell morphologies on undeformed and deformed HA and PEI/HA-coated Mg after culturing for 5 days: HA coated Mg samples (A) before deformation and (B) after 5% deformation. HA-PEI coated Mg samples (C) before deformation and (D) after 5% deformation.

Chapter 3.

Ta/PEI coating on Magnesium implants to enhance corrosion resistance and biological properties for orthopedic applications

3.1 Introduction

Currently, there is an increasing demands for biodegradable materials that can be degraded without toxicity for many biomedical applications [36, 68, 70, 100]. Previously, commercial metallic implants, Ti or CoCr alloys, have been used for many kinds of biomaterials, such as load-bearing or vascular stent applications, owing to their excellent biocompatibility and mechanical strength. However, they can cause stress shielding effect and permanent inflammation, which results in requiring secondary removal surgery after tissue healing process [101]. Therefore, magnesium and its alloys have been promising and actively researched due to its superior mechanical properties compared with other biodegradable polymers or ceramics [92]. Magnesium is known to have similar mechanical properties with human bones, which can reduce the stress shielding effect. Furthermore, during corrosion process, by-products from Mg are rarely detrimental to human body. Especially, Mg ions, which are released during the corrosion process, would be used for metabolism of cells [3, 17, 36, 102]. However, due to the poor corrosion resistance of magnesium, corrosion occurs too rapidly in the physiological conditions, and the mechanical properties for supporting are attenuated before tissue regeneration. In addition, hydrogen gas or hydroxide ions released during the corrosion process may interfere with the regeneration of surrounding tissues, which can lead to tissue

necrosis or failure of implantation if even worse [19, 20, 103].

Thus, in order to utilize magnesium for various medical fields, it is imperative to improve the corrosion resistance to modulate the rapid corrosion rate. For this purpose, alloying with other elements or surface treatment has been performed to improve the corrosion resistance in the previous research [36, 70, 104]. Among various methods to mitigate intrinsic fast corrosion rate of Mg alloy, the surface coatings are being considered as the most effective methods to be able to enhance corrosion resistance and biocompatibility, depending upon biomaterial on the surface. Of the various surface coating, metallic or ceramic coatings have the several advantages because of relatively high corrosion resistance and superior biocompatibility. Still, these coatings are susceptible to external deformation, which leads to failure of coating layer and discourages the corrosion resistance. Polymer coatings, on the other hand, are advantageous in that they are not susceptible to deformation due to their flexible nature and thus can be extensively used in various medical fields [84, 93, 105]. Among various polymer coating materials, poly (etherimide) (PEI) polymer is known as a promising coating material due to its high corrosion resistance, excellent mechanical properties, high adhesive strength and biocompatibility compared to other biodegradable polymers [80, 106, 107]. However, PEI has low bioactivity and is known to have less osteoconductivity than other

bioceramics. In order to overcome the problem, PEI-based composite coating system have been developed using bioceramics, such as silica or hydroxyapatite particles, to improve bioactivity [108, 109]. Nevertheless, this composite system has a problem in that corrosion resistance of the coating layer may deteriorate as depending on the amount of incorporated particle and biocompatibility can be influenced by the distribution of particles [105]. Therefore, there is a need for research to improve the biocompatibility and bioactivity through the surface treatment of the coating layer while maintaining the corrosion resistance of the coating layer.

S-PIII is the most promising and innovative method of polymer surface treatment. Briefly, based on sputtering system, a high negative bias is applied to a substrate, to which metal ions are to be implanted, so that the metal ions emitted from the metal target are accelerated and implanted onto the polymer surface (**Figure 3.1**). It has the advantage of shortening the process time and metallizing the polymer surface without any special interface [110, 111]. By applying this technique to polymer coating layer on magnesium, metal ions are implanted into the extremely thin surface of the polymer coating layer with nano-scale while maintaining the corrosion resistance of the coating layer, thereby the biocompatibility can be improved considerably. The chosen metal target is tantalum (Ta), which has excellent corrosion resistance, superior

biocompatibility, bioactivity, osteoconductivity and been widely used as biomedical applications [112, 113]. By implanting accelerated tantalum ions into the extreme surface layer of the PEI coating layer through the S-PIII technique, the surface properties of the coating layer are modified. It contributes to improvement of coating function, exhibiting superior biocompatibility and bioactivity compared to conventional PEI coatings.

In this study, we studied the corrosion resistance and biocompatibility of Ta ion implanted PEI coating on magnesium surface. Firstly, PEI of 2μm was coated on the surface, and then a high negative bias of -2000V was applied to the specimen and sputtering-based Ta ion implantation process was performed. The surface and cross-sectional morphologies were confirmed by SEM and TEM, and the chemical characteristics of the surface were confirmed by XPS and wettability. In order to investigate the effect of Ta ion implantation on corrosion resistance, the volume of evolved hydrogen gas was measured and the volume change of the specimens was monitored as corrosion time went by. Finally, we evaluated improvement of Ta ion implantation into the PEI coating layer *in vitro* and *in vivo* analysis using pre-osteoblast and rabbit femur models.

3.2 Material and methods

3.2.1 Material preparation

Mg alloy WE43 (yttrium (4.1 wt.%), neodymium (2.1 wt.%), zirconium (0.56 wt.%), manganese (0.028 wt.%), and balance Mg; Yueyang Yuhua Yejin company, China) was used as a model Mg substrate for the present work because of its wide use in orthopedic applications. Each specimen was prepared with the dimensions of 10 mm x 10 mm x 2 mm and polished using abrasive SiC paper up to 2000 grit and were cleaned with ethanol in an ultrasonic bath. As shown in **Figure 3.2**, PEI pellets were dissolved in N-methyl-2-pyrollidone (NMP, Sigma–Aldrich, USA) at a concentration of 15% w/v and stirred at 37°C for overnight. The PEI solution was spin-coated on the Mg substrate at 2000 rpm for 1 min and the coated samples were dried at 70°C for 1 day to remove residual solvent and densify PEI coating layer. After PEI coating and drying, the coated specimens were placed in a vacuum chamber. A tantalum target (diameter 75mm, thickness 5 mm, purity 99.99%, Kojundo Chemical Lab, Japan) was placed in a DC magnetron sputter gun housing (Ultech Co. Ltd., Korea). After a chamber was pumped to 5×10^{-4} Pa using rotary pump and diffusion pump, the PEI-coated Mg specimens were applied to S-PIII technique with Ta target under high negative voltage of 2000 V for 30 seconds while 7 mTorr of Ar gas flow. Target current was applied with 50mA

and no additional heat was applied [110]. The PEI-coated Mg, which was applied with Ta ion implantation, was referred to as the Ta/PEI-coated Mg.

3.2.2 Characterization of the Ta/PEI-coated Mg

The surface morphologies of the bare Mg, the PEI-coated Mg and the Ta/PEI-coated Mg were observed with field-emission scanning electron microscopy (FE-SEM; MERLIN Compact, ZEISS, Germany) and the thickness of the PEI coating layer was confirmed by FE-SEM and focused ion beam (FIB). The surface roughness of the bare Mg, the PEI-coated Mg, and the Ta/PEI-coated Mg was assessed by atomic force microscopy (AFM; PAFM NX, EM4SYS Co., Ltd., Korea) under the non-contact mode; the size of the characterized region was 10 × 10μm. The cross-sectional view of the Ta/PEI coating layer was exhibited with a transmission electron microscope (TEM; JEM-2100F, JEOL, Japan) and the element linear profile was evaluated by energy dispersive x-ray spectroscopy (EDS) analysis affiliated with TEM. Mechanical stability of Ta implanted PEI coating on Mg was confirmed by observing surface morphology with FE-SEM, compared to Ta coated PEI coating on Mg. The experimental condition of Ta coated PEI coating, sputtering time was about 5 min under low negative voltage of 200 V. To evaluate mechanical performance of the Ta/PEI coating layer, a 10% tensile strain

deformation was applied to the samples using Instron tensile machine (Instron 5582) at a rate of 5mm/min. The surface chemistry of the PEI-coated Mg and the Ta/PEI-coated Mg was evaluated by X-ray photoelectron spectrometer (XPS; Axis Supra^{TM}, Kratos, England). The hydrophilicity of the bare Mg, the PEI-coated Mg, and the Ta/PEI-coated Mg was analyzed by measuring contact angle using a distilled water droplet using the Phoenix 300 contact angle analyzer (Surface Electro Optics Co., Ltd., Korea). In addition, the longevity of the modified surface under dry and wet conditions was evaluated by immersion in a phosphate-buffered saline (PBS) solution for one week. The contact angle was calculated with ImageJ program (National Institutes of Health, Bethesda, USA).

3.2.3 *In vitro* Corrosion behavior of the Ta/PEI-coated Mg

The corrosion behavior was evaluated by monitoring the amount of evolved hydrogen (H_2) gas during corrosion after the bare Mg, the PEI-coated Mg, and the Ta/PEI-coated Mg were placed in simulated body fluid (SBF) at a temperature of 37°C for 10 days. The SBF was prepared according to the method suggested by Kokubo et al. [90]. Before immersion in SBF, the uncoated side of the Mg samples was mounted using epoxy resin. From the amount of H_2 gas, the *in vitro* corrosion rate was calculated based on the

following stoichiometry:

$$Mg + 2H_2O \rightarrow Mg(OH)_2 + H_2$$

The volume change of the Mg cylinder was monitored with micro computed tomography (μ-CT; Skyscan 1173, Konitch, Belgium) at day 0, 3, 6, and 14 under the following conditions: a resolution of 18 μm using a 1-mm aluminum filter, a voltage of 130 kV, and a current of 60 mA. Before the corrosion test, a Mg cylinder was prepared from the WE43 ingot with a diameter of 4 mm and a length of 6 mm. The samples were polished with 2,000 SiC paper and cleaned with ethanol. Following the cleaning process in ethanol with ultrasonic bath, the PEI was coated onto the Mg cylinder using a dipping machine at a withdrawal speed of 1 mm/min. The coating procedure was repeated twice and the Mg cylinder was dried at 70℃ overnight. After the PEI coating, the S-PIII technique was conducted under the same conditions as the substrate samples; both ends of the Mg cylinder were mounted with epoxy resin. After all samples were immersed in the SBF, the morphologies and volume of the cylinder were confirmed and calculated using commercial analysis software (CTAn, Bruker, Belgium) for 14 days, and the 3D structural images of the corroded samples were obtained using post-processing software (CTVox, Bruker, Belgium).

3.2.4 *In vitro* biological properties of the Ta/PEI-coated Mg

The initial cell attachment, proliferation and differentiation of the pre-osteoblast cell (MC3T3-E1; CRL-2593, ATCC, USA) was evaluated on the bare Mg, the PEI-coated Mg and the Ta/PEI-coated Mg. The cells were cultured in an alpha minimum essential medium (α-MEM, welgene Co., Korea) supplemented with 10% fetal bovine serum (FBS) and 1% penicillin-streptomycin in a humidified incubator with 5% CO_2 at 37℃. Before in vitro cell test, all samples were cleaned with ethanol and dried in a vacuum chamber overnight. And then, they were placed in clean bench to sterilize with ultraviolet light for 1 day.

The initial cell attachment was observed using confocal laser microscopy (CLSM; LSM710, Carl Zeiss, Germany) after culturing 6 h and 24 h with seeding density of 3×10^4 cells/ml on the bare Mg, the PEI-coated Mg and the Ta/PEI-coated Mg. After culturing for 6 h and 24 h, the samples were washed with Phosphate-buffered Saline (PBS, pH 7.4; WELGENE Inc., Korea) and stained with Live/Dead assay (L3224, Invitrogen, Carlsbad, USA) for 30 min in the dark.

The cell proliferation of pre-osteoblast cells on the bare Mg, the PEI-coated Mg and the Ta/PEI-coated Mg was evaluated by measuring the DNA amount of the attached cells on the samples using a Cyquant cell proliferation

assay kit (C7026, Invitrogen, Carlsbad, USA) after culturing for 1 day, 3 days and 5 days with a density of 3×10^4 cells/ml. After the cells were seeded, the culture medium was refreshed every day. After culturing at a predetermined time, the cells adhered on the samples were detached using 0.25% Trypsin-EDTA for 4 min at 37℃ and suspended in a fluorescent dye solution. The DNA level of the detached cells was measured using a multiple plate reader (Victor3, Perkin Elmer, Germany). The excitation and emission wavelength were 495 and 520 nm during measurement, respectively.

Cell differentiation of pre-osteoblast cells on the bare Mg, the PEI-coated Mg and the Ta/PEI-coated Mg was performed using an alkaline phosphatase (ALP) activity assay after culturing for 10 days with a density of 0.5×10^4 cells/ml. After 1 day, 10mM β-GP and 50 mg/ml ascorbic acid were added to the culture medium for accelerating the cell differentiation and the culture medium was refreshed every 3 days. The ALP activity was examined at a wavelength of 405 nm using a micro reader (Model 550, Biorad, USA). The number of the samples was three specimens for each condition. The number of the samples were three samples, respectively.

3.2.5 Evaluation of *in vivo* biodegradation and bone response

New Zealand white rabbits (10-week-old, 2.8-3.0 kg, kosabio, Korea)

were used for evaluating the *in vivo* bone response and biodegradation of the bare Mg, the PEI-coated Mg and the Ta/PEI-coated Mg cylindrical samples (**Figure 3.3**). The preparation method of the sample was same as mentioned in 3.2.3. The *in-vivo* animal tests were approved by the Institutional Animal Care and Use committee of Genoss (GEN-IACUC no. 1811-03). The *in-vivo* animal experiments were carried out using the rabbit femoropatellar groove model [114-116]. All rabbits were anesthetized by an anesthetic mixture with 0.7 ml of 2% Xylazine HCl (Rompun, Bayer Korea, Korea), 1.4 ml of Tiletamine HCl (Zoletil, Virbac Laboratories, France), and 0.5 ml of Lidocaine (Yuhan Corporation, Korea) administered by intramuscular injection. Following anesthetization, a cylindrical hole (4 mm in diameter and 6 mm in length) was formed in femoral groove parallel to the long axis of femur with a hand drill. The bare Mg, the PEI-coated Mg and the Ta/PEI-coated Mg cylindrical sample were implanted individually into femur defect of each rabbit.

The rabbits were sacrificed after 4 week of implantation. The corroded volume of each Mg samples and the total bone formation around Mg samples were measured by scanning the harvested bone tissues and the specimens using micro-CT with a 1.0mm aluminum filter at a resolution of 17μm, a voltage of 130kV and a current of 60μA. The 3D and 2D images of the samples and bone tissues were reconstructed with post-processing software (NRecon and Data

Viewer 1.4, Skyscan). The corroded volume and the bone formation volume were quantified using commercial analysis software (CTAn, Skyscan) with processed micro-CT images and the 3D images of the samples and the bone were acquired using post-processing software (CTvox, Skyscan). The three samples of each type were used to attain mean and standard deviation. The in-vivo degradation rate was calculated from equation. (ΔV : volume change, A : initial surface area of the sample, t : implantation time)

$$\text{Degradation rate (mm/year)} = \frac{\Delta V}{At}$$

After micro-CT imaging, the extracted regions were fixed in 10% formaldehyde and embedded in resin (Technovit 7200 VLC, Kulzer, Germany). These resin block containing samples were sectioned to a thickness of <50μm with grinding system (Exakt, Germany). Histological sections were stained by haemotoxylin-eosin (H&E) and analyzed using Axioskop microscopy (Olympus BX51, Olympus Corporation, Japan).

3.2.6 Statistical analysis

All data were presented as the mean ± standard deviation. Statistical package for the social sciences (SPSS 23, SPSS Inc., U.S.A) software was conducted for the statistical analysis. Normality of the variables were verified

with Shapiro-Wilk test and the statistical analysis were carried out by one-way analysis of variance (ANOVA) with Tukey post-hoc comparison. A p value less than 0.05 was supposed statistically significant in all cases.

3.3 Results and discussion

3.3.1 Characterization of the Ta/PEI-coated Mg

The surface morphologies and roughness were presented in **Figure 3.4**. The bare Mg showed distinct grinding grooves distributed evenly throughout the surface (**Figure 3.4Aa**), whereas a completely smooth surface morphologies were observed on the PEI-coated and Ta/PEI-coated Mg without any noticeable surface defects (**Figure 3.4Ab and c**). As shown in insets b and c, both coating layers had an almost identical thickness of 2 μm and were uniformly coated on the surface of Mg with a good interfacial adhesion to the Mg substrate. The surface roughness of the samples was similar tendency with SEM images, as shown in **Figure 3.4B**. The average surface roughness of the bare Mg (R_a = 33.2 ± 7.2 nm) was about 25.5 and 19.5 times higher than those of the PEI-coated (R_a = 1.3 ± 0.3 nm) and Ta/PEI-coated Mg (R_a = 1.7 ± 0.6 nm), respectively (**Table 3.1**), and there is no statistical difference between the PEI-coated and Ta/PEI-coated Mg ($p > 0.05$). The cross-sectional view and line EDS results of Ta/PEI-coated Mg were exhibited in **Figure 3.5**. As shown in **Figure 3.5A**, Ta implanted layer was shown brighter than other polymer part because heavier atoms, such as tantalum atoms, scatter electrons more than lighter atoms, such as carbon atoms of polymer coating. The implanted thickness and the contents of Ta ions was about 10 nm and 15~20 at% (**Figure**

3.5B). As the tantalum fraction increases, the fraction of oxygen increases as well, suggesting that the implanted tantalum ions reacted with the surrounding oxygen in the air and exist in the form of tantalum oxide.

Mechanical stability of Ta implanted PEI coating was identified with dog-bone shape specimens under tensile deformation, compared to Ta coated PEI coating (**Figure 3.6**). As shown **Figure 3.6A**, the surface morphology of Ta implanted PEI coating showed negligible change after applying tensile deformation. In contrast, many cracks were found at the surface of Ta coated PEI coating, as observed in **Figure 3.6B**. In the Ta implanted PEI coating, any interface was not existed as shown in **Figure 3.5A** because Ta ions were implanted gradually into polymeric matrix due to high accelerating force induced by high negative voltage. Therefore, Ta implanted PEI coating could maintain its biological functions under dynamic conditions. However, Ta coating on PEI matrix formed overall interface between Ta deposited layer and PEI coating. The presence of this interface could act as a crack initiator under tensile deformation because strain is distributed throughout the interface. Therefore, propagation of cracks occurs and eventually causes failure of deposited Ta layer. If such unstable layer is present in biological environment, it could be detached from the implants and hardly enhance biocompatibility or hemo-compatibility consistently and effectively.

Chemical composition of the samples was examined by XPS analysis (**Figure 3.7 and Table 3.2**). As shown in **Figure 3.7A and B**, the PEI-coated Mg showed representative peaks of the PEI chemical structure, including spectra of Carbon (C 1s), Oxygen (O 1s) and Nitrogen (N 1s), and the peaks of Mg (Mg 2p and KLL) was completely diminished. After Ta ion implantation, the metallic Ta peaks, such as Ta 4f, Ta 4d, Ta 4p, were identified at the spectra of the Ta/PEI-coated Mg, as displayed in **Figure 3.7C**. From the high resolution of Ta 4f peak as shown in inset of **Figure 3.7C** (top-right inset in Figure 3.7C), high intensity peaks of Ta_2O_5 at binding energies of 26.3 and 28.3 eV [117] and low intensity peaks of Ta^0 at 21.5, and 23.4 eV were observed [118]. It indicates implanted Ta ions were reacted with oxygen in air, which result is consistent with the result of line EDS analysis, as shown **Figure 3.4B**. Generally, Ta_2O_5 is known for stable state of tantalum, which suggests functionality of PEI coating layer can improve stably under various physiological conditions. Furthermore, metal oxide, such as $Mg(OH)_2$, and imide ring of PEI molecule have strong interaction [119]. It also implements implanted Ta ions exist, showing good stability at the molecular level.

The surface wettability of the bare, PEI-coated, and Ta/PEI-coated Mg was characterized by measuring contact angle with distill water on their surface. Their surface wettability, one of the most important material properties

affecting cell adhesion, growth, and tissue development. As shown in **Figure 3.8**, the PEI coating layer formed on the Mg surface (PEI-coated Mg) significantly led to increased surface hydrophobicity with a contact angle of 79.3 ± 1.1°, which correspond well to the previously published data [73], although the surface of bare Mg had reasonable hydrophilicity with a contact angle of 40.8 ± 3.6°. In contrast, the Ta/PEI-coated Mg surface showed a similar wettability to the bare Mg, showing a contact angle of 49.5 ± 5.9°; this surface hydrophilicity remained almost constantly for 7 days under both air and PBS immersion conditions (**Figure 3.8B**), which indicated surface hydrophilicity by Ta incorporation could be representing for a long time, regardless of environment. However, in the wet condition, the bare Mg was rapidly corroded, forming porous corrosion by-products, such as $Mg(OH)_2$ and MgO, its water contact angle continuously decreased down to 12.3 ± 2.8° with increasing immersion time.

3.3.2 *In vitro* corrosion behavior of the Ta/PEI-coated Mg

Corrosion behavior of the bare Mg, the PEI-coated Mg and the Ta/PEI-coated Mg was evaluated in SBF to verify the effect of Ta ion implantation technique in terms of corrosion resistance. Firstly, the amount of evolved hydrogen gas from Mg substrate was measured and in vitro corrosion rate was

calculated, as shown in **Figure 3.9**. As shown in **Figure 3.9A**, the amount of hydrogen gas from the bare Mg was much larger than that of the PEI-coated Mg specimens, which indicates PEI coating layer prevented direct contact effectively between Mg surface and aqueous solution or electrolyte. Also, delamination of coating layer by formation of hydrogen gas pocket at the interface was suppressed by strong adhesion strength between Mg and PEI, resulting in sustaining high corrosion resistance. After Ta ion implantation, the amount of evolved hydrogen gas was similar to before Ta ion implantation. Although the hydrophilicity of the PEI coating layer was better by implanted Ta, corrosion resistance of the PEI coating layer seemed to be hardly affected because the thickness of Ta implanted region was about 15 nm, which was about 1/100 of the thickness of entire coating layer. Typically, polymeric coating layers effectively suppress high reactivity of Mg thermodynamically controlling a rate-determining step of overall corrosion reaction. In particular, hydrophobic and dense polymer matrices substantially retard the penetration of corrosive medium into the Mg substrate, which plays the slowest step within all corrosion kinetic processes, and, consequently, decreases the corrosion rate. Even though the Ta ion implantation altered the surface physical and chemical properties of the PEI coating, the Ta-implanted layer had only a few tens of nanometers, and that is probably too shallow to alter the overall corrosion protection property of the PEI coating. In addition, the Ta ion implantation

process may damage the polymer chains on the coating surface while tantalum oxide, which is known to be highly corrosion resistive material, was packed between polymer chain, which can suppress the penetration of the surrounding water or electrolyte through polymer chain. As a result, the overall corrosion resistance appeared to have no significant effect by combining these effects. For quantitative comparison, *in vitro* corrosion rate (mm/year) was converted using the result of the amount of evolved hydrogen gas, as presented in **Figure 3.9B**. In the case of the bare Mg, the corrosion rate was about 5.08 ± 0.89 mm/year, showing corrosion occurred severely. However, the corrosion rates of the PEI- and the Ta/PEI-coated samples were about 1.16 ± 0.75 mm/year and 1.09 ± 0.58 mm/year, respectively and their corrosion rates were significantly decreased compared to that of the bare Mg. Before and after Ta ion implantation, *in vitro* corrosion rate was very similar to each other, indicating the Ta implanted PEI coating can serve as corrosion resistive layer, effectively.

Figure 3.10 shows the structural morphologies and quantitative volume change of cylindrical Mg samples with μ-CT analysis at a predetermined time. As shown **Figure 3.10A**, the bare Mg was corroded severely and quickly even for 3 days and the site of pitting corrosion was found. As corrosion went by in SBF, corroded area became larger and corroded part was found at entire surface at 14 days. However, the morphology of the PEI-

coated Mg cylindrical sample was maintained and pitting corrosion part was found not until 14 days. Alike the result of the amount of evolved hydrogen gas (**Figure 3.9**), the morphology of the Ta/PEI-coated Mg cylindrical sample was similar to the PEI coated sample. Quantitative volume change of the samples was presented as shown in **Figure 3.10B**. The bare Mg was corroded continuously and linearly until 14 days and remaining volume of the bare Mg cylinder was about 81.84 ± 7.37%. The PEI-coated Mg samples were quantitatively confirmed to show a much smaller corroded volume than the bare Mg and the volume of 96.8 ± 5.53% remained after 14 days, indicating that the corrosion rate was much slower. After Ta ion implantation, it was found that 95.93 ± 1.59% of initial volume remained until 14 days. Furthermore, the volume change of the samples was also converted quantitatively to corrosion rate, as observed in **Figure 3.10C**. These value were similar to corrosion rate derived by evolved hydrogen gas, as mentioned in **Figure 3.9B**. As a result, it was considered that the corrosion resistance was not significantly changed before and after the Ta ion implantation technique. From the results of corrosion behavior, Ta implanted PEI coating improved strongly the corrosion resistance of uncoated Mg and it does not have a significant effect on the performance of the polymer coating layer even though high negative bias was applied to the PEI-coated Mg sample. In previous research, there were some attempts to improve corrosion resistance by coating tantalum on the Mg surface or by

implanting tantalum ions. It has been reported that ZK60 alloy was coated with tantalum to improve the corrosion resistance, or the corrosion resistance is improved by implanting Ta ion to the Mg surface by using the conventional ion immersion implantation technique for AZ31 or Al-Mg alloy [120-122]. Yet, in the case of simple coating, if unexpected delamination or defect at the coating layer occurs, galvanic corrosion occurs at the exposed interface, and there is a possibility that the corrosion rate becomes faster [123]. In addition, most of these studies have only confirmed short-term corrosion behavior, and galvanic corrosion or unexpected corrosion behavior may be caused by implanted metallic components when they are present in the body for a long period of time. However, in this study, since tantalum metal ion was implanted into the PEI polymeric layer, magnesium and bioactive metal are not in direct contact with each other and there is little possibility of unexpected galvanic corrosion, which suggests Ta implanted PEI coating can increase corrosion resistance of magnesium implant for long-term period.

3.3.3 *In vitro* biocompatibility of the Ta/PEI-coated Mg

In order to *in vitro* biocompatibility, attachment, proliferation and differentiation of pre-osteoblast cells were evaluated, including the bare Mg, the PEI-coated Mg and the Ta/PEI-coated Mg. **Figure 3.11** presents the CLSM

images of adhered pre-osteoblast cells on the Mg samples with Live/Dead assay after culturing for 6 h and 24 h. As shown in **Figure 3.11A**, pre-osteoblast seeded on the bare Mg appeared to be adhered to the surface with spherical shape. However, as shown in **Figure 3.11A**, it was observed that some filopodia of pre-osteoblast cells on the PEI-coated Mg. After Ta ion implantation, most of the pre-osteoblast cells showed multiple filopodia and they were attached to the surface more extensively and actively compared to those on the PEI-coated Mg (**Figure 3.11E)**. After culturing for 24 h, pre-osteoblast cells attached on the bare Mg has a spherical shape similar to 6 h (**Figure 3.11B)**. Because the bare Mg was corroded rapidly in the medium and generated hydrogen gas inhibited cell adhesion, continuously. In addition, due to the hydroxyl ions generated during the corrosion process, the medium was alkalized, resulting in creating an unfavorable environment to the pre-osteoblast cells [89]. However, it was confirmed that pre-osteoblast cells attached on the PEI-coated Mg showed larger area relative to bare Mg, and that after Ta ion implantation, most of the cells were flattened and much more filopodia than those on the PEI-coated Mg (**Figure 3.11D and F)**. The PEI coating layer inhibited the initial corrosion and facilitated cell attachment compared to bare Mg. However, the PEI coating does not exhibit sufficient cellular response compared to the Ta/PEI-coated Mg because it has relative hydrophobic nature without any special receptor that promote cell attachment. However, after the Ta ion

implantation, the pre-osteoblast cells seemed to be flattened and stretched shape, having much more multiple filopodia unequivocally compared to the PEI-coated Mg because the metalized surface of the coating layer facilitated the initial attachment of the cells. Generally, cells recognize the surface of implant material through filopodia, such as receptor or biomolecules on the surface, which results in changing its morphologies through various information about the surface that is collected by sensing and signaling with filopodia [124]. On the Ta/PEI-coated Mg, the relatively larger number of filopodia was found, which means that there is an interaction between the cell and the surface of the material occurs actively and considerably [125]. As a result, adhesion of cell-material is facilitated, affecting to cell proliferation and differentiation positively. **Figure 3.12A and B** show the DNA amount and ALP activity of pre-osteoblasts cultured on bare Mg, PEI-coated Mg, and Ta/PEI-coated Mg. Cell proliferation was assessed by measuring DNA amount of pre-osteoblast after culturing for 1, 3, and 5 days on the bare Mg, PEI-coated Mg, and Ta/PEI-coated Mg, as shown in **Figure 3.12A**. In the first day, the DNA level of pre-osteoblasts cultured on the PEI-coated Mg and Ta/PEI-coated Mg was higher than that of pre-osteoblast on the bare Mg. As exhibited in **Figure 3.11**, it is believed that the number of cells was smaller than that of the coated specimens since generated hydrogen gas suppressed the initial attachment of cells. In the 3 days and 5 days, the DNA level of the pre-osteoblasts cultured on Ta/PEI-

coated Mg was much higher than that of bare Mg and PEI-coated Mg. As presented in **Figure 3.11**, it is considered because it provided a more favorable environment for cell growth. Quantitatively, the amount of DNA on the Ta/PEI-coated Mg increased about 590% and 160% more than that of bare Mg and PEI-coated Mg, respectively at 3 days. In addition, at 5 days, the amount of DNA on the Ta/PEI-coated Mg was as high as 343% and 162% compared to the bare Mg and the PEI-coated Mg, indicating that cell proliferation was actively induced in Ta/PEI-coated Mg. **Figure 3.12B** shows ALP activity of pre-osteoblasts cultured on the bare, the PEI-coated and Ta/PEI-coated Mg. After culturing for 10 days, the ALP activity of pre-osteoblasts cultured on Ta/PEI-coated Mg was significantly higher than that of PEI-coated Mg. Such improvement in *in vitro* biological properties are closely related to the physicochemical properties of the coating layer [125, 126]. First, due to the higher corrosion resistance of the PEI coating layer, the pre-osteoblasts were adhered better on the PEI coating layer compared to the bare Mg because an environment for cell proliferation is established. In addition, tantalum is implanted into the surface of the coating layer due to the Ta ion implantation, so that it is possible to easily provide the binding site to the cell due to the relatively improved hydrophilicity. It is known that the higher the hydrophilicity, the more easily the medium or nutrients required for cell growth can be accessed, which also achieve a significant effect on cell adhesion and growth

[108, 127-130]. In addition, tantalum itself is known as a material with excellent biocompatibility and bioactivity, thus providing a better environment for cell growth than a carbon-based synthetic polymer [131].

3.3.4 *In vivo* biodegradation and bone response

In order to confirmed the *in vivo* biodegradability and osteogenetic capability of the materials, cylinder-shaped bare, PEI-coated, and Ta/PEI-coated Mg samples were implanted in both sides of femoropatellar defects of each rabbit, and after implanting for 4 weeks, implanted samples and trabecular bones around the sample were characterized by micro-CT. As shown in **Figure 3.13**, the 2D coronal and transverse images of the implanted samples clearly represent an adverse biological impact of the bare Mg implant (**Figure 3.13A and B**); there are extremely large voids around the implant surfaces, and surrounding trabecular bone tissues were completely separated from the implant surface, leaving the implant almost unfixed in the host femur because the bare Mg corroded most rapidly. The rapid corrosion led to continuous evolution of H_2 gases and hydroxyl ions on its surface, which resulted in forming several large voids around the bare Mg implant [89]. However, relatively smaller voids were observed around the PEI-coated Mg and the Ta/PEI-coated Mg, compared to the bare Mg, which resulted from improved

corrosion resistance by introducing surface coating. In particular, it was confirmed that the Ta/PEI-coated specimen had a larger contact area with surrounding bone. **Figure 3.14** shows the shape and volume of the bone formed around the cylindrical specimens. As shown in **Figure 3.14**, the surface of the cylindrical bare Mg was covered by the formed bone relatively much smaller compared to PEI coated specimens, and the exposed surface was relatively larger. In the case of the Ta/PEI-coated specimen, it was confirmed that covered surface was much larger than the bare Mg and the PEI-coated Mg. **Figure 3.15** shows the ratio of corroded volume of the Mg samples after 4 weeks. The bare Mg was corroded about 10% over a period of 4 weeks, and the corroded volume of the PEI- and the Ta/PEI-coated specimens was about 4% of initial volume. In the case of the bare Mg, corrosion rate was much faster than the PEI-coated specimen because it was directly in contact with the body fluids and chloride-containing electrolyte. However, the PEI-coated Mg was found to show a relatively low corrosive volume due to increasing the corrosion resistance by inhibiting direct contact of the body fluids with the Mg scaffold. There was almost no discrepancy between the PEI-coated Mg and the Ta/PEI-coated Mg similar to *in vitro* corrosion test. Quantitatively, *in vivo* corrosion rate of the bare Mg was about 1.31 ± 0.27 mm/year, and the corrosion rates of the PEI-coated Mg and the Ta/PEI-coated Mg were 0.58 ± 0.22 mm/year and 0.49 ± 0.02 mm/year, respectively. It indicates that the Ta implantation process for 30

seconds and Ta implanted region on PEI coating layer hardly affected to the corrosion resistance of the PEI coating layer, as in the previous *in vitro* corrosion test. The calculated *in vitro* corrosion rate was faster about 2 to 4 times than the *in vivo* corrosion rate. This discrepancy between *in vitro* and *in vivo* corrosion rate has been explained in other many research about Mg. Firstly, chloride ions, which is the most critical ions in corrosion of Mg, dissolved in SBF or Hank's solution used in *in vitro* corrosion test are larger than the actual amount of chloride ions dissolved in body fluids or blood. Secondly, protein or amino acid as well as inorganic ions were dissolved in actual body fluids or blood. Thus, it is known that these organic components have the effect of reducing the overall corrosion rate by interfering with the dissolution of the magnesium oxide layer [68]. The total bone volume around the bare, the PEI-coated and the Ta/PEI-coated Mg was exhibited in **Figure 3.16**. As observed in **Figure 3.14**, Quantitatively, the total bone volume was about 3.67 ± 0.16 mm^3, 4.72 ± 1.32 mm^3 and 7.01 ± 0.41 mm^3, around the bare, PEI- and Ta/PEI-coated Mg, respectively. Furthermore, the amount of bone formed around Ta/PEI-coated Mg was 1.9 times and 1.48 times much larger than that of bare and PEI-coated Mg, individually. *In vivo* biological response is strongly influenced by the corrosion resistance of Mg and the surface characteristics of the coating material, as well as the results of *in vitro* cell test. During corrosion of bare Mg, hydrogen gas was generated around the specimen, which makes it difficult to

adhere the cells and the releasing hydroxyl ions from the Mg sample led to the tissue regeneration around implants due to the local alkalization [89]. Furthermore, new bone formation can be inactivated by large amount of released Mg ions [78, 132]. On the contrary, the Ta/PEI-coated Mg showed the highest bone formation compared to the bare and PEI-coated Mg. Owing to Ta implanted PEI coating, hydrogen gas and hydroxide ions were released little and enhanced hydrophilicity facilitated cell adhesion and assessment of fluid or nutrient, which results in accelerating regeneration of bone compared to bare Mg [89, 127, 133, 134]. Histological images for the bare, PEI-coated, and Ta/PEI-coated Mg implants are shown in **Figure 3.17;** in which the longitudinally sectioned each implant was stained with Goldner's trichrome and displayed with low and high magnifications. Mineralized and matured bone appeared in dark green, latest formed but still unmineralized bone (osteoid) in orange, and Mg implant in light green (for corrosion product) and black (for not yet corroded matrix). Overall, the bare Mg implant showed severely corroded surface features with more corrosion products deposited along the specimen's surface in comparison to both the coated Mg implants. In particular, as indicated by voids in **Figure 3.17Aa–c**, there is noticeable histological appearance of the vigorous hydrogen gas evolution surrounding the bare Mg implant, which leads to the complete separation of the trabecular bone from the implant surface. In case of the PEI-coated and Ta/PEI-coated Mg implants,

there is no appreciable corrosion on its surface or void formation around the implant with the low magnification (**Figure 3.17Ba and Ca**); at high magnification histological photograph, only little amounts of corrosion products are exhibited, partially covering its surface (**Figure 3.17Bb–c and Cb–c**). However, while many regions of the trabecular bone in the distal femur were located at certain distances from the surface of the PEI-coated Mg, developing the tissue-free voids around the implant, the Ta/PEI-coated Mg implant continued to tightly adhere to the adjacent bone tissue, and more portion of its surface was surrounded by the trabecular bones rather than the voids. In addition, much of the mineralized and unmineralized bones could be found in direct-contact and near-contact regions to the Ta/PEI-coated Mg implant surface, compared to the bare or PEI-coated Mg implants. These *in vivo* results clearly demonstrates the excellent corrosion protection ability of the PEI coating as well as the osseointegration ability of the Ta-implanted coating surface layer. Without the PEI coating, the bare Mg corroded rapidly; its surface was rough with thick corrosion byproducts (**Figure 3.17A**). However, direct bone-to-implant contact did not occur on the surface of the PEI-coated Mg implant (**Figure 3.17B**). Since the primary function of orthopedic implants is to support mechanical interlocking and replace the biological function of bone, it is not possible to achieve appropriate early fixation as well as long-term implantation success in the absence of direct bonding. As shown in **Figure**

3.17C, among the three samples, the Ta/PEI-coated Mg implant saw direct bone-to-implant contact at the microscopic level. Furthermore, the highest level of total bone volume around the Ta/PEI-coated Mg implant surface was found, specifically 194% and 149% higher than that of the bare and PEI-coated Mg implants, respectively (**Figure 3.15 and 16**), which can mainly be attributed to the presence of Ta on the surface. Ta forms hydroxide groups on the surface within body fluids, which subsequently attracts calcium and phosphate ions near the surface and ultimately results in the formation of apatite layers. In conclusion, based on the outstanding corrosion protection ability and biological activity, the Ta/PEI-coated Mg implant has promoted affinity and fixation with surrounding bone tissue and osseointegration capability at the early stage of bone healing process, which can prevent failure of material, as shown in **Figure 3.18**.

3.4 Conclusions

In this study, we introduced an innovative approach to modify physical and chemical properties of the surface of the polymeric coating on Mg implant. The PEI-coated Mg showed outstanding corrosion protective ability, which resulted from the hydrophobic property of PEI coating layer and its strong adhesion strength to the Mg surface. However, their osseointergration ability

was not proved with the surrounding bone. A rapid PIII technique combined with DC magnetron sputtering, termed as S-PIII, made it possible to inject much better biocompatible Ta ions into the surface of PEI coating layer with an extremely short processing time (30 s). After S-PIII treatment, surface morphology or corrosion protection of the Ta/PEI-coated Mg was not damaged or attenuated. Moreover, Ta-implanted PEI layer could be sustained its surface morphology under tensile deformation of 10%, which indicates Ta-implanted PEI coating showed considerably physical and chemical stability. Rather, a generated nano-thick Ta-implanted layer of 15~20 nm on the topmost PEI surface led to significantly improved surface hydrophilicity and long-lasting longevity under both dry and wet conditions. Owing to Ta's bioactivity and biocompatibility, the Ta/PEI-coated Mg facilitated initial attachment, proliferation and differentiation of pre-osteoblasts as compared to the bare and PEI-coated Mg. In *in vivo* rabbit femur study, the Ta/PEI-coated Mg implant presented promoted bone tissue affinity and osseointegration capability without any signs of appreciable Mg corrosion. These results demonstrate that the Ta/PEI-coated Mg implant has tremendous potential for biodegradable orthopedic implant applications, which resulted from suggesting early mechanical fixation as well as long-term implantation effects.

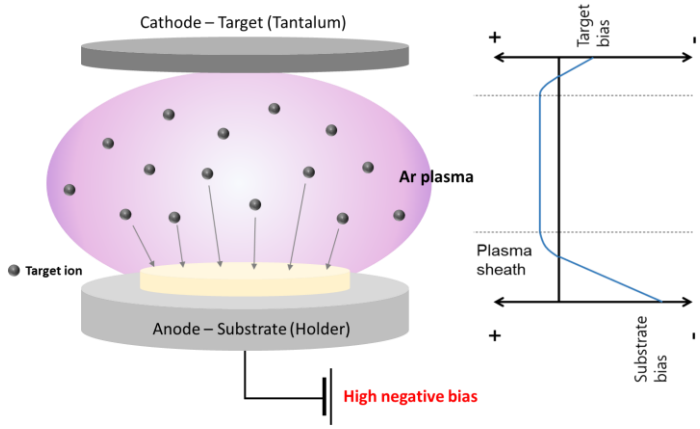

Figure 3.1 Schematic diagram of S-PIII technique.

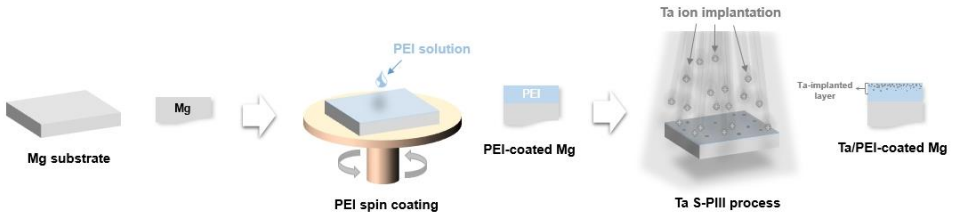

Figure 3.2 Experimental procedure for Ta implanted PEI coating on Mg substrate.

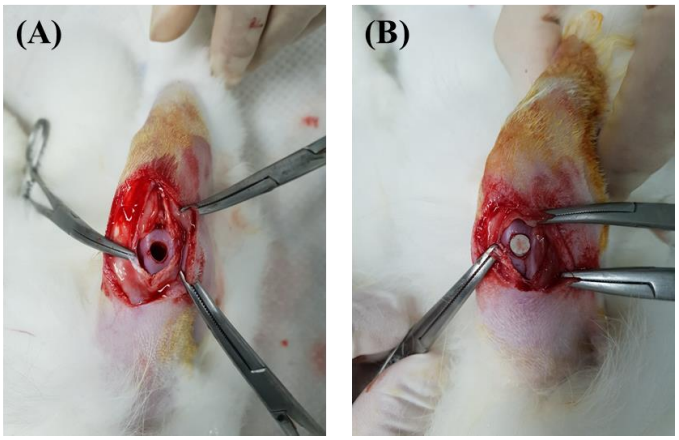

Figure 3.3 *In-vivo* rabbit femoropatellar groove model experiment (A) before and (B) after implantation of Mg cylindrical sample.

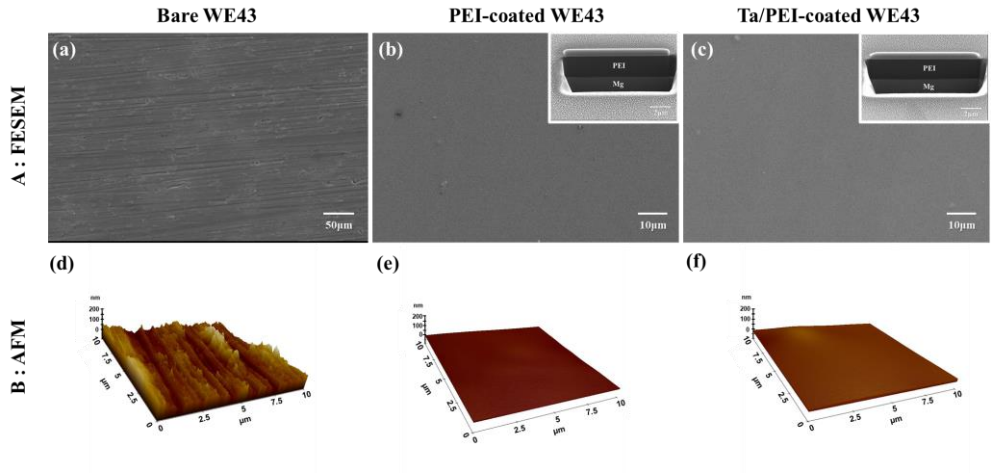

Figure 3.4 (A) Surface morphologies and (B) representative AFM topographical images of (a,d) the bare Mg, (b,e) the PEI-coated Mg and (c,f) the Ta/PEI-coated Mg (inset : cross-sectional images).

Sample	R_a (nm)	R_q (nm)	R_z (nm)
Bare Mg	33.23 ± 7.18	42.8 ± 9.83	335.2 ± 70.44
PEI-coated Mg	1.33 ± 0.32	1.8 ± 0.48	17.08 ± 2.82
Ta/PEI-coated Mg	1.7 ± 0.65	2.18 ± 0.82	15.8 ± 5.69

Table 3.1 Surface roughness of bare, PEI coated and Ta/PEI-coated Mg.

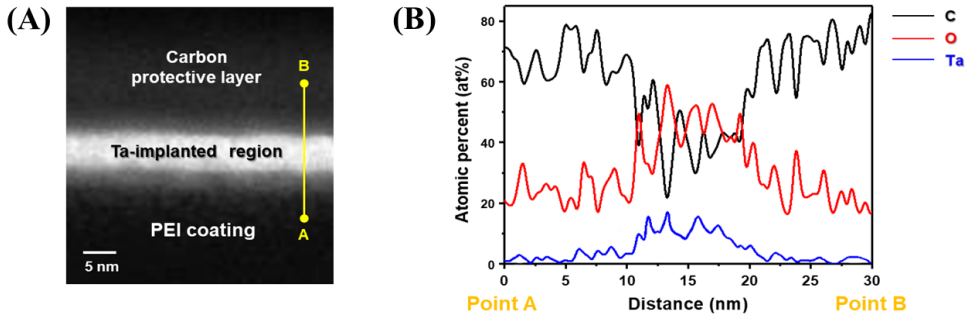

Figure 3.5 (A) High-resolution cross-sectional STEM image of Ta/PEI-coated Mg and (B) STEM/EDS compositional profiles of C (black), O (red), and Ta (blue) through the yellow line from point A to B shown in (A).

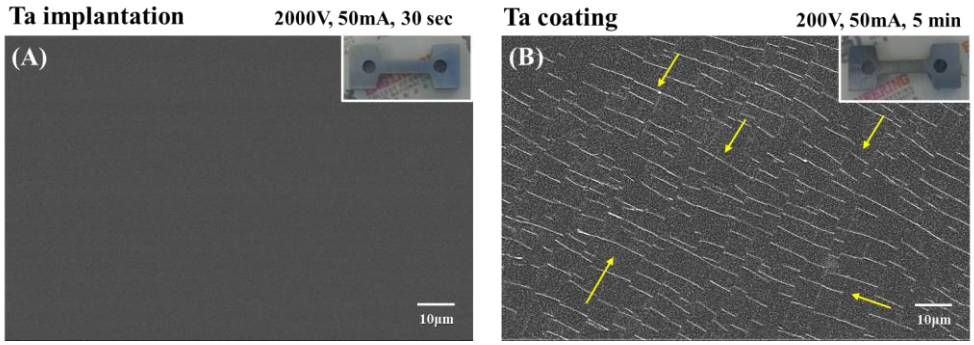

Figure 3.6 Surface morphologies of (A) the Ta implanted PEI coating, and (B) Ta coated PEI coating on dog-bone shaped WE43 substrate after 10% deformation with strain rate of 5mm/min.

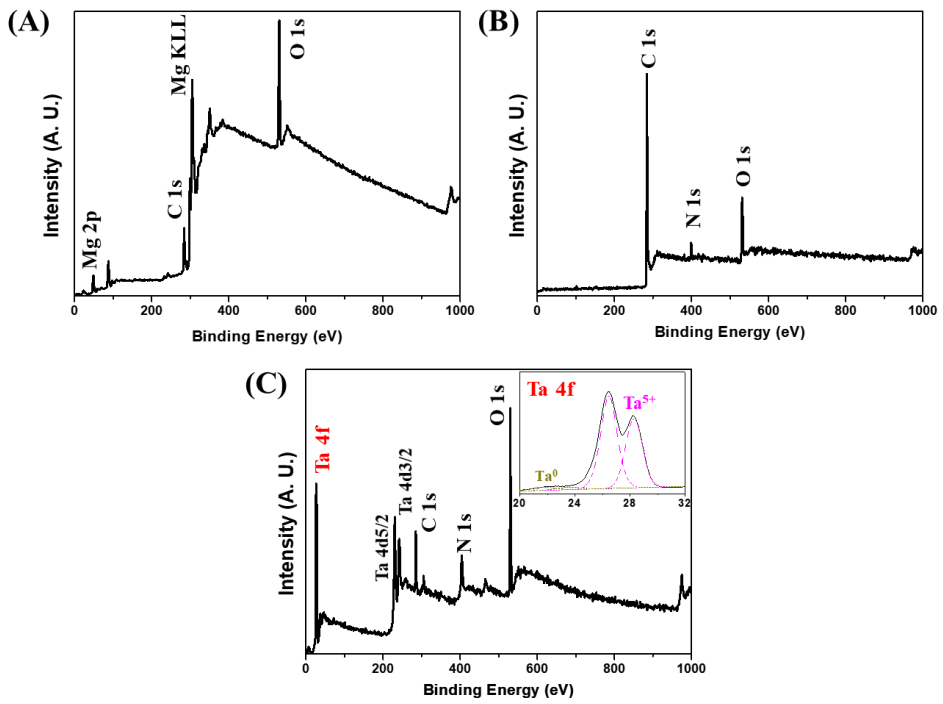

Figure 3.7 XPS spectra of (A) the bare Mg, (B) PEI-coated Mg and (C) Ta/PEI-coated Mg (Inset: Ta 4f XPS spectra).

Sample	Atomic concentration (%)				
	Magnesium	Carbon	Oxygen	Nitrogen	Tantalum
Bare Mg	22.9	35.5	41.6	-	-
PEI-coated Mg	0.2	73.5	24	2.3	-
Ta/PEI-coated Mg	0.9	42	47	-	10.1

Table 3.2 XPS analysis: Elemental atomic concentrations of the samples.

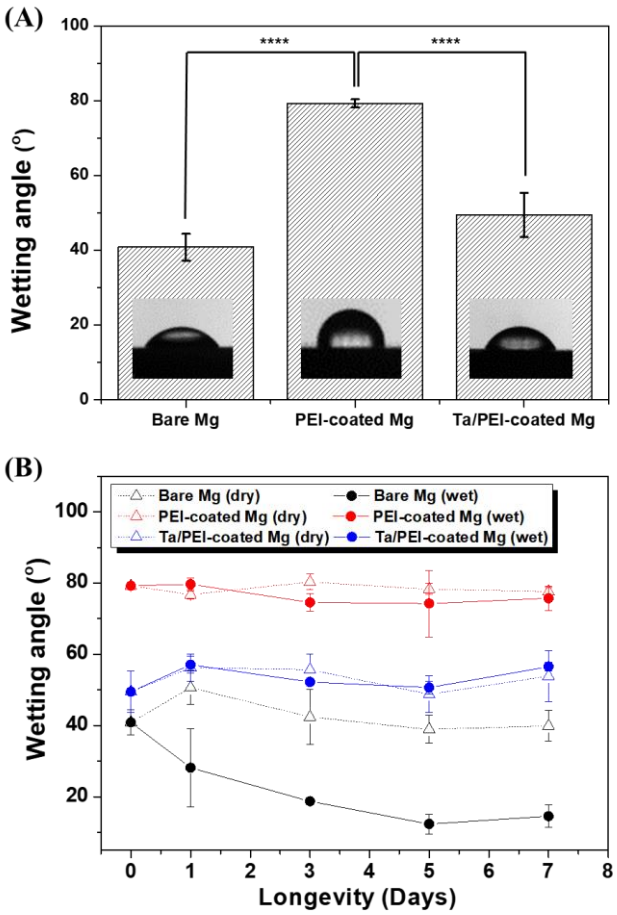

Figure 3.8 (A) Water contact angles of bare, PEI-coated, and Ta/PEI-coated Mg samples and (B) their longevities as a function of time under air and distilled water immersion conditions.

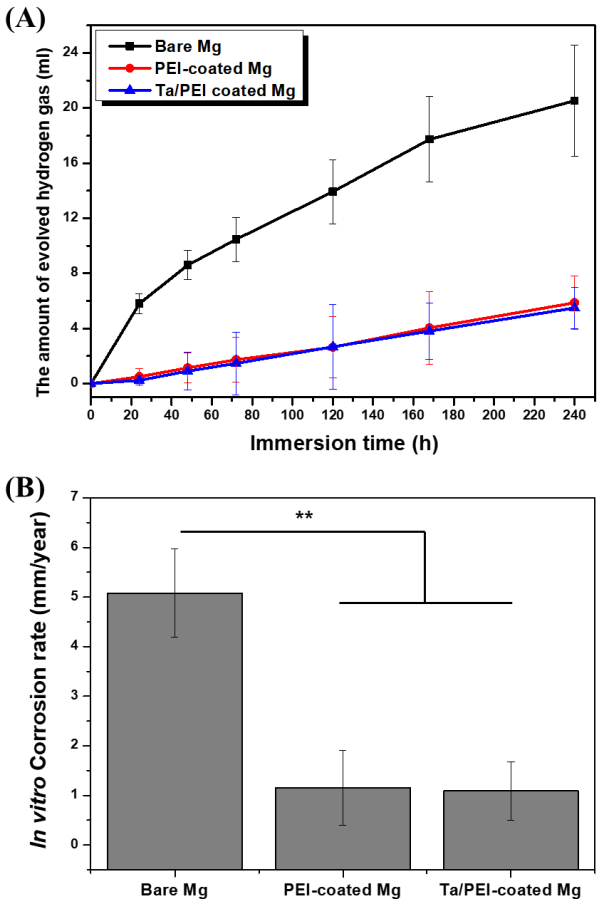

Figure 3.9 (A) The graph of evolved H_2 gas amount in SBF solution of the bare Mg, the PEI- and Ta/PEI- coated Mg after immersion in SBF solution for 10 days (B) and the calculated *in vitro* corrosion rate of each Mg sample (**p < 0.01).

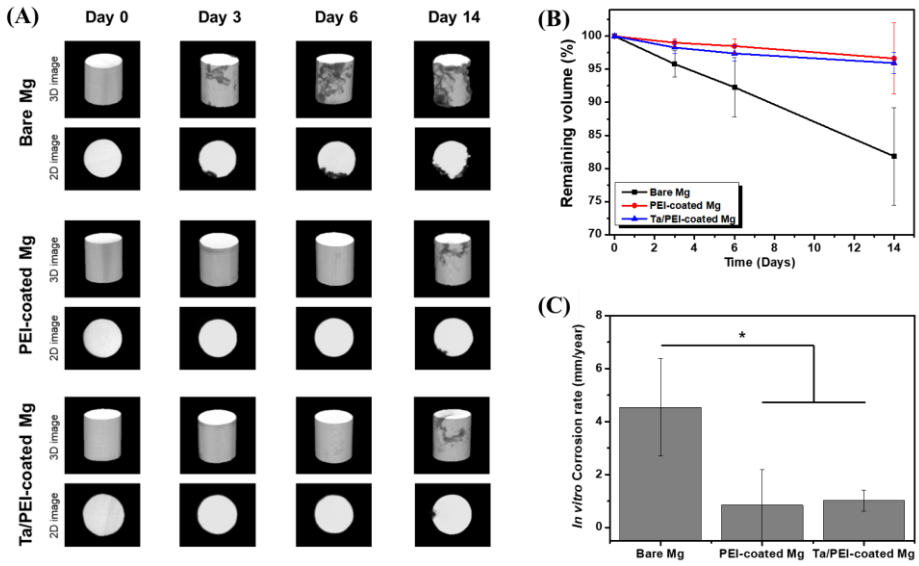

Figure 3.10 (A) 3D images of the bare, PEI- and Ta/PEI-coated Mg at 0, 3, 6, and 14 days of immersion and their (B) remaining volumes. (C) Their calculated corrosion rates. Statistical significance is indicated by *$p < 0.05$.

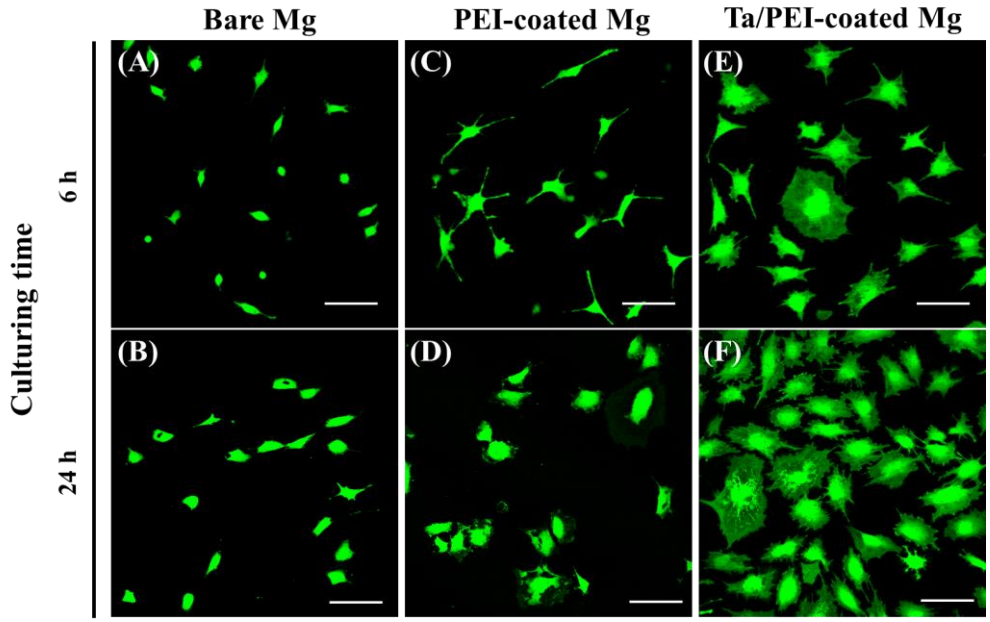

Figure 3.11 CLSM images of adhered MC3T3-E1 cells on the surface of (A)–(B) bare, (C)–(D) PEI-coated Mg, and (E)–(F) Ta/PEI-coated Mg after culturing for 6 and 24 h (scale bar: 100 μm).

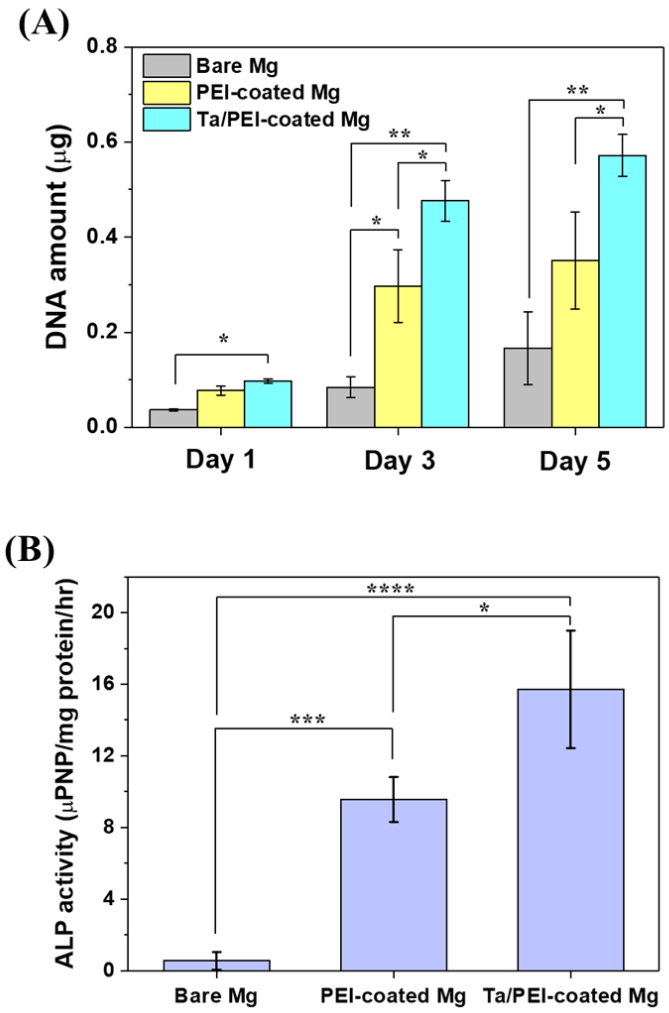

Figure 3.12 (A) DNA amount and (B) ALP activity of MC3T3-E1 cells on the bare, PEI- and Ta/PEI-coated Mg after culturing for 1, 3, and 5 days and 10 days, respectively (*$p < 0.05$, **$p < 0.01$, ***$p < 0.005$, and ****$p < 0.001$).

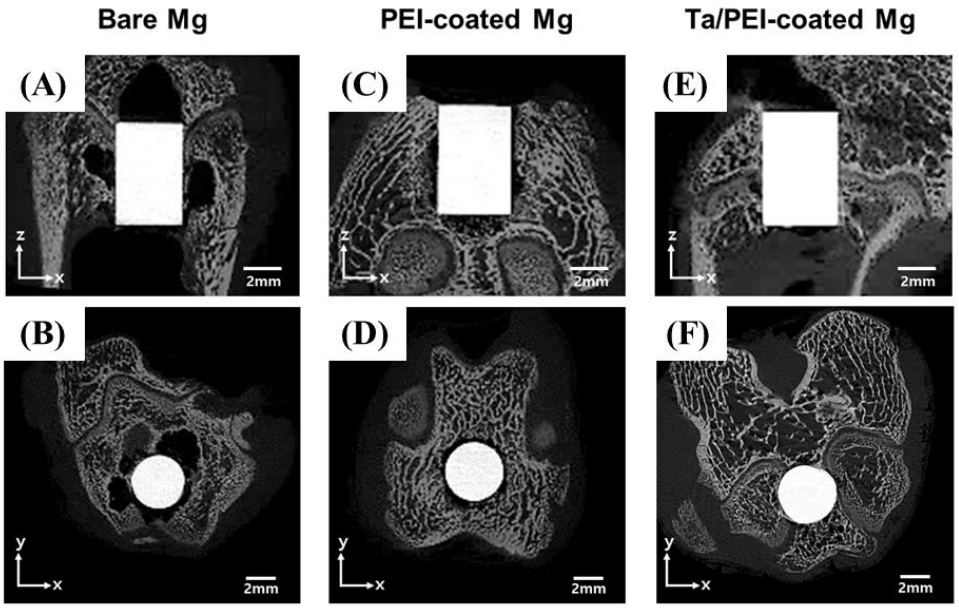

Figure 3.13 Cross-sectional 2D coronal and transverse μ-CT images of each implants after implantation for four weeks, (A)-(B) bare Mg, (C)-(D) PEI-coated Mg and (E)-(F) Ta/PEI-coated Mg sample.

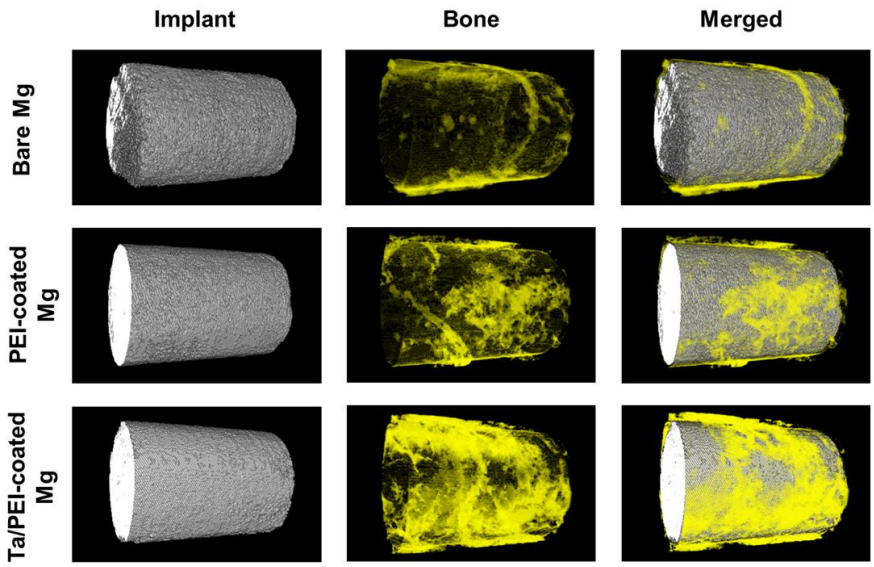

Figure 3.14 3D re-constructed images of bone tissue and the bare Mg, the PEI-coated Mg and the Ta/PEI-coated Mg implant after 4 weeks (gray : specimen, yellow : bone)

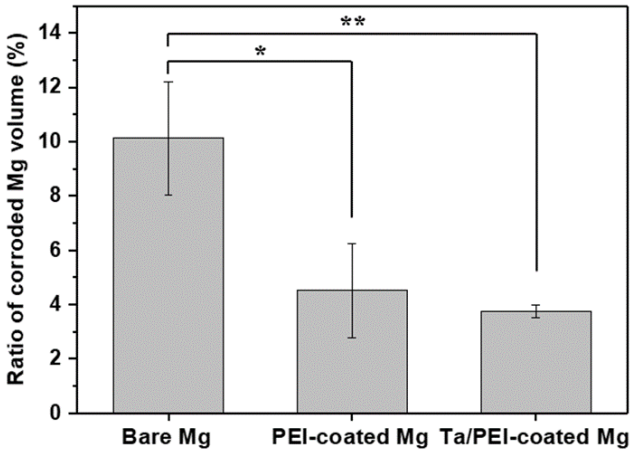

Figure 3.15 The graph of corroded volume of the bare Mg, the PEI-coated Mg and the Ta/PEI-coated Mg after 4 weeks (*$p < 0.05$, **$p < 0.01$).

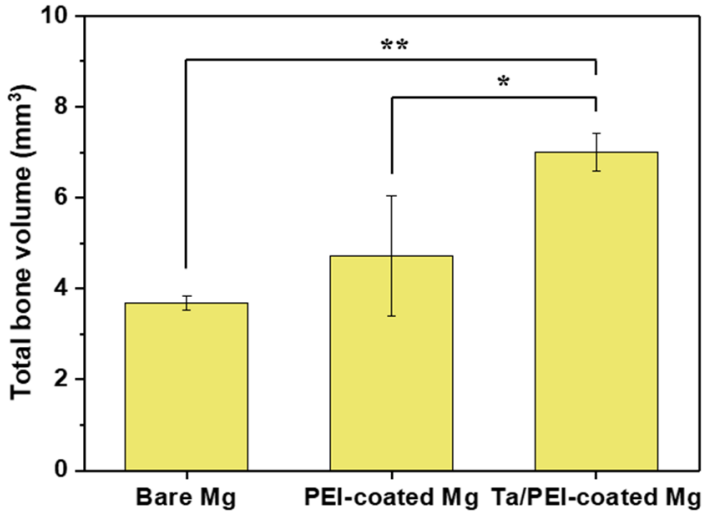

Figure 3.16 The graph of total bone volume within a defined region around the bare Mg, PEI-coated Mg and Ta/PEI-coated Mg after 4 weeks (*$p < 0.05$, **$p < 0.01$).

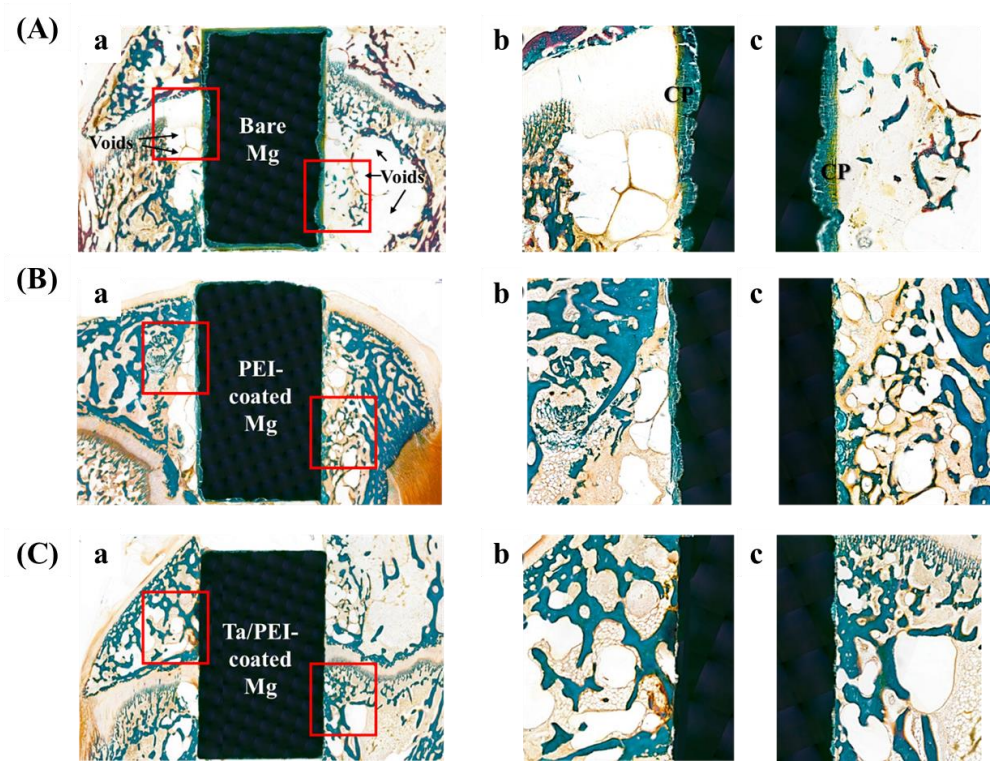

Figure 3.17 Representative histological images of (A) bare, (B) PEI-coated, and (C) Ta/PEI-coated Mg implants with (a) low and (b)–(c) high magnifications around the Mg samples regions in a rabbit femur 4 weeks after implantation. Magnified regions are highlighted with red rectangles in relatively low-magnification images.

Figure 3.18 Schematic diagram of bone healing process at early stage along with the degradation of Ta/PEI-coated Mg scaffold.

Chapter 4.

Conclusion

4.1 Conclusion

In this thesis, we developed functional surface coating for Mg-based implant that fulfills the two main requirements necessary to the practical use of such biodegradable devices, namely a high corrosion resistance and biocompatibility. In addition to them, deformable surface coatings were developed because various mechanical deformation occurs in the real medical situations.

In Chapter 2, after introducing groove patterns on the magnesium surface, a selective ceramic-polymer coating was developed, which could retain its function even under tensile strain. In order to improve the corrosion resistance of Mg, many studies have been extensively conducted to improve corrosion resistance and biocompatibility by coating a bio-ceramic material on the Mg surface. However, such bioceramic coatings cause cracking and delamination of the coating layer when a certain amount of deformation is applied due to the brittleness of the ceramic material itself, which resulted in exposing the Mg surface to physiological environment. Then, despite the presence of coating layer, the corrosion rate and biocompatibility cannot be maintained since local corrosion began from the exposed Mg surface. In order to suppress the occurrence of such defects, micro-scale groove patterns were introduced on the Mg surface to control the strain distribution generated during

deformation according to the surface topography. Depending on the groove patterns on the surface, little strain was applied to the top parts of the groove patterns, while the strain was concentrated to the bottom parts of the groove patterns. Based on this distribution, HA was coated on ‘hill part’ where tensile strain was rarely applied, and the flexible PEI that can withstand high strain was coated in the inner 'valley part' of the groove where the strain is concentrated. The appropriate size of the groove patterns was determined through Abaqus, a representative software of Finite Element Analysis (FEA). Based on this, a uniform groove pattern having a size of approximately 20μm was produced using laser machining on the Mg surface. With the patterned Mg samples, PEI was spin-coated to fill the valley part of the groove, and then HA was coated on the hill part of the groove through hydrothermal process. The developed HA-PEI coated Mg with micropatterns, unlike the existing HA coating layer, was able to maintain its surface morphology even at a tensile strain of 5% without any cracks or delamination. It indicated Mg surface is not exposed due to no defect in the HA coating layer. As a result of *in vitro* corrosion test, it was confirmed that the HA coated Mg, was corroded rapidly after deformation, while the HA-PEI coating layer retains high corrosion resistance even before and after deformation. In addition, as a result of the initial cell attachment experiment using pre-osteoblast, the adhesion of cells on the HA coating layer was disturbed by evolved hydrogen gas after tensile

deformation due to the rapid corrosion of Mg, but on the HA-PEI coating layer, cells were attached well to the surface both before and after deformation. In conclusion, the HA-PEI coating layer developed by introducing the groove pattern showed its functions that maintaining outstanding corrosion resistance and biocompatibility even in various deformation occurring in the actual medical environment.

Therefore, in order to solve this limitation, Ta metal ions implanted into the surface of the polymeric coating layer using sputtering system to improve biocompatibility and bioactivity. Firstly, PEI coating was coated on the Mg surface, and then the S-PIII process using a DC magnetron sputter was performed for about 30 seconds to inject Ta metal ions. The S-PIII process is a process in which metal ions emitted from a metal target are injected into a polymer surface by applying high negative voltage to a specimen to be implanted. Compared to the previous P-III process, the process time is significantly shortened, which has the advantage of reducing damage that may occur in the polymer coating layer. After the S-PIII process, it was confirmed that the polymer coating layer retained their morphology without any specific defects, and Ta implanted region with content of 10-15 at% was formed with a thickness of 15-20nm on the topmost of polymeric coating surface. In addition, since this Ta-rich region did not form any special interface with the existing PEI

coating layer. By interface-free layer, the surface morphology of Ta/PEI-coated Mg was maintained even when 10% tensile strain was applied. The chemical state of implanted Ta was found in the form of tantalum oxide, reacting with oxygen and it is found that the hydrophilicity of the polymer coating layer was greatly improved, and maintained for a long time even in wet conditions. In the *in vitro* corrosion test through monitoring of evolved hydrogen gas and specimen volume change for a predetermined time, the corrosion resistance of Ta/PEI-coated Mg was much higher than that of the non-coated Mg and not significantly different from that of PEI-coated Mg. It implied that the Ta metal ion implantation through the S-PIII process does not significantly affect the corrosion resistance of the PEI coating layer. Additionally, the *in vitro* cell test confirmed that Ta/PEI-coated Mg facilitated cell adhesion and promotes proliferation and differentiation significantly, compared to bare Mg and PEI-coated Mg. Ta was implanted into the polymer surface, which remarkably improved the hydrophilicity, making it easier to attach the cells, and thus, the cell-materials interaction was actively conducted, which seemed to enhance biological performance. *In vivo* test results also showed that the corrosion rate of Ta/PEI-coated Mg was the slowest, as well as the affinity with surrounding bone tissue was much higher than other conditions.

This study suggests that HA-PEI coated Mg with micropatterns and

Ta/PEI-coated Mg offered an attractive potential for biodegradable devices. Depending on these applications, the HA-PEI coating and Ta/PEI coating can improve the functions of the Mg-based implants by increasing the corrosion resistance and biocompatibility under various mechanical deformation. Therefore, the study emphasized the functional surface coatings to be able to apply Mg-based biodegradable medical devices.

4.2 Future Works

In the thesis, functional coatings have been introduced to improve corrosion resistance and biocompatibility even under deformation. Based on these approaches, we are suggesting the possible future possibility of research and investigations.

From chapter 2, groove pattern was introduced to the Mg surface in order to redistribute the strain applied on the surface. In this study, a 1-dimensional groove pattern was fabricated to conduct an experiment under tensile deformation with one-direction, but if it is manufactured as a 2-dimensional pattern, as shown in **Figure 4.1**, a HA-PEI coating platform can withstand not only tensile deformation but also bending deformation. It is also believed that these groove patterns can be used not only for Mg but also for other deformable metal materials, such as Ti and Co-Cr. Furthermore, this groove pattern can be used not only as a coating platform, but also as a platform to modulate cellular response. On this pattern, attachment, movement and growth of the cells would be caused along with the topography of pattern, thereby promoting osteoblast differentiation or actively inducing endothelization. On the basis of these advantages, polymer material with groove pattern on the surface can be fabricated by using the groove patterned metal stamp. Such a polymer material may be used for a GBR membrane or

artificial vessel.

From chapter 3, Ta implanted PEI coating could be introduced for vascular stent applications. Ta implanted polymeric surface could enhance hemo-compatibility as well as biocompatibility. Therefore, we introduced Ta/PEI coating system into Mg stent. As shown **Figure 4.2**, Ta ions were implanted into luminal side of the PEI coated Mg stent using a DC magnetron sputter. Likewise, Ta implanted region was fabricated on the topmost of PEI coating layer and this region could influence drug release behavior, endothelization and platelet activation. Due to Ta implanted region of about 10-15 nm, release rate of drug loaded in PEI coating was decreased (**Figure 4.3**) Furthermore, on the surface of the Ta/PEI-coated Mg, endothelization was occurred rapidly and platelet adhesion and activation was suppressed, which indicated possibility of in-stent restenosis and late-stent thrombosis could be reduced by improved biocompatibility and hemo-compatibility (**Figure 4.4 and 4.5**). In conclusion, this Ta/PEI coating can be applied to various biomedical applications.

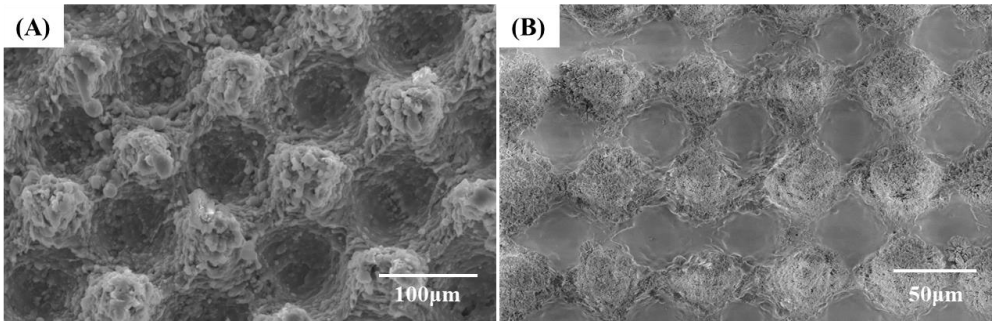

Figure 4.1 The surface morphologies of (A) bare Mg and (B) the HA-PEI coated Mg with 2-dimensional groove pattern

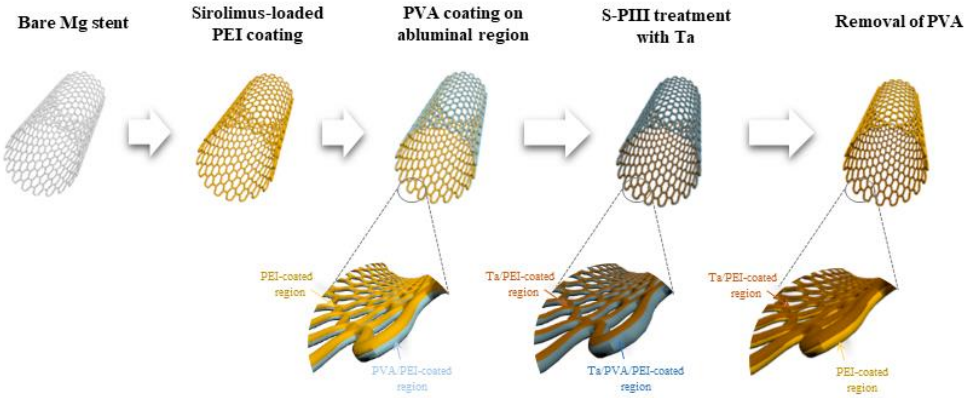

Figure 4.2 Schematic diagram of experimental methods of Ta/PEI-coated Mg stent

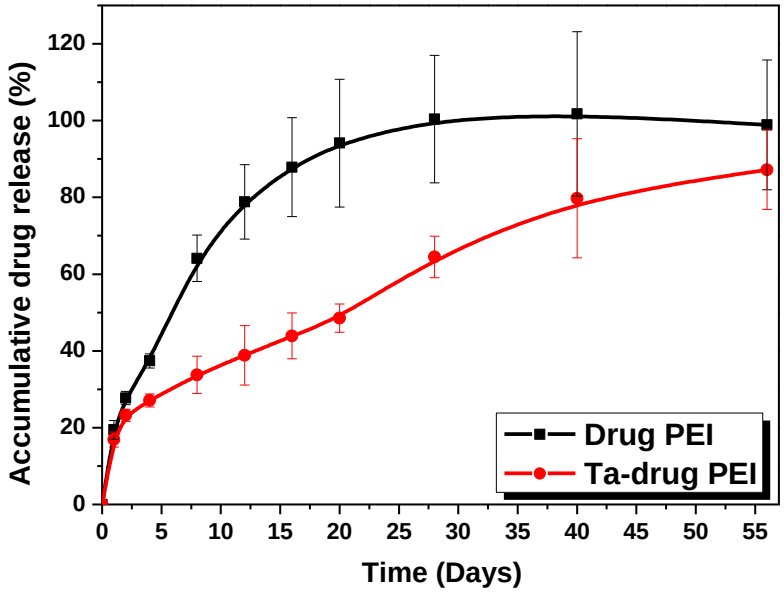

Figure 4.3 Sirolimus release profile for 8 weeks from PEI-coated and Ta/PEI-coated Mg substrate with sirolimus in tween-20 containing PBS solution.

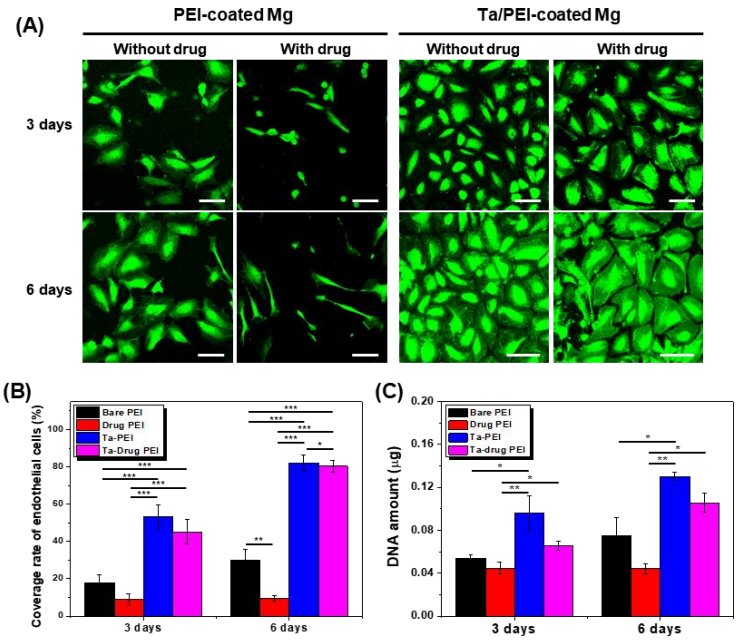

Figure 4.4 (A) Representative CLSM images of adhered endothelial cells on the PEI-coated and Ta/PEI-coated Mg with and without drug after culturing time for 3 and 6 days. (scale bar : 100μm) (B) Surface coverage rate and (C) DNA amount of endothelial cells cultured on the PEI-coated and Ta/PEI-coated Mg with and without drug (*$p < 0.05$, **$p < 0.01$, ***$p < 0.005$)

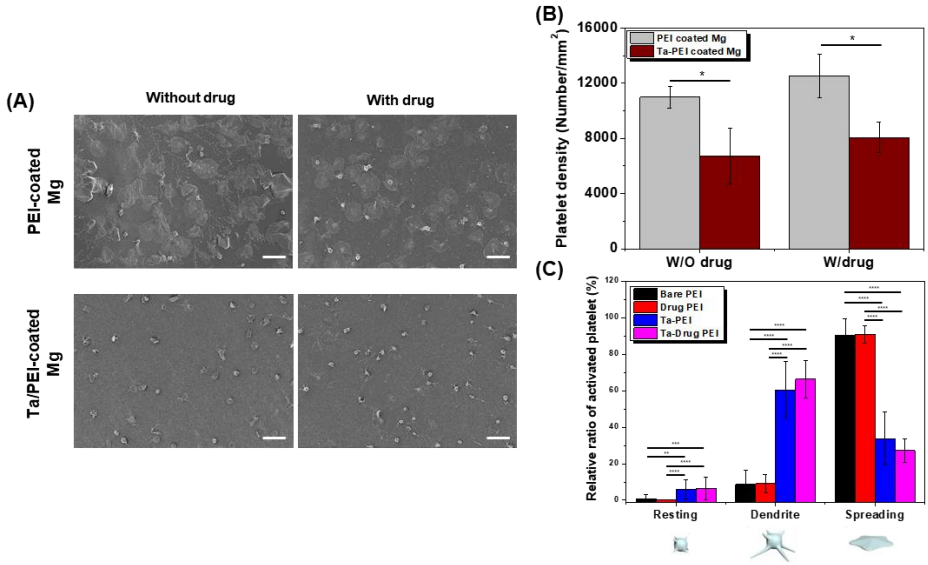

Figure 4.5 (A) Representative FE-SEM images of adhered platelet on the PEI-coated and Ta/PEI-coated Mg with and without drug after culturing time for 1 hour (Scale bar : 10μm). (B) Quantitative density of adhered platelet and (C) the ratio of the activated platelet cultured on the PEI-coated and Ta/PEI-coated Mg with and without drug (*p < 0.05, **p < 0.01, ***p < 0.005, ****p<0.001)

References

[1] N.S. Manam, W.S.W. Harun, D.N.A. Shri, S.A.C. Ghani, T. Kurniawan, M.H. Ismail, M.H.I. Ibrahim, Study of corrosion in biocompatible metals for implants: A review, Journal of Alloys and Compounds 701 (2017) 698-715.

[2] G. Reith, V. Schmitz-Greven, K.O. Hensel, M.M. Schneider, T. Tinschmann, B. Bouillon, C. Probst, Metal implant removal: benefits and drawbacks--a patient survey, BMC Surg 15 (2015) 96.

[3] D. Zhao, F. Witte, F. Lu, J. Wang, J. Li, L. Qin, Current status on clinical applications of magnesium-based orthopaedic implants: A review from clinical translational perspective, Biomaterials 112 (2017) 287-302.

[4] A.M.S. Ibrahim, P.G.L. Koolen, K. Kim, G.S. Perrone, D.L. Kaplan, S.J. Lin, Absorbable Biologically Based Internal Fixation, Clin Podiatr Med Sur 32(1) (2015) 61-+.

[5] B.D. Ulery, L.S. Nair, C.T. Laurencin, Biomedical Applications of Biodegradable Polymers, J Polym Sci B Polym Phys 49(12) (2011) 832-864.

[6] M. Navarro, A. Michiardi, O. Castano, J.A. Planell, Biomaterials in orthopaedics, J R Soc Interface 5(27) (2008) 1137-58.

[7] H. Liu, E.B. Slamovich, T.J. Webster, Less harmful acidic degradation of poly(lactic-co-glycolic acid) bone tissue engineering scaffolds through titania nanoparticle addition, Int J Nanomed 1(4) (2006) 541-545.

[8] R. Zeng, W. Dietzel, F. Witte, N. Hort, C. Blawert, Progress and Challenge for Magnesium Alloys as Biomaterials, Advanced Engineering Materials 10(8) (2008) B3-B14.

[9] J. Nagels, M. Stokdijk, P.M. Rozing, Stress shielding and bone resorption in shoulder arthroplasty, J Shoulder Elb Surg 12(1) (2003) 35-39.

[10] J.E. Gray, B. Luan, Protective coatings on magnesium and its alloys - a critical review, Journal of Alloys and Compounds 336(1-2) (2002) 88-113.

[11] F.I. Wolf, J.A. Maier, A. Nasulewicz, C. Feillet-Coudray, M. Simonacci, A. Mazur, A. Cittadini, Magnesium and neoplasia: from carcinogenesis to tumor growth and progression or treatment, Arch Biochem Biophys 458(1) (2007) 24-32.

[12] J.L. Wang, J.K. Xu, C. Hopkins, D.H.K. Chow, L. Qin, Biodegradable Magnesium-Based Implants in Orthopedics—A General Review and Perspectives, Advanced Science (2020).

[13] D. Zhao, S. Huang, F. Lu, B. Wang, L. Yang, L. Qin, K. Yang, Y. Li, W. Li, W. Wang, S. Tian, X. Zhang, W. Gao, Z. Wang, Y. Zhang, X. Xie, J. Wang, J. Li, Vascularized bone grafting fixed by biodegradable magnesium screw for treating osteonecrosis of the femoral head, Biomaterials 81 (2016) 84-92.

[14] J. Wang, J. Xu, B. Song, D.H. Chow, P. Shu-Hang Yung, L. Qin, Magnesium (Mg) based interference screws developed for promoting tendon graft incorporation in bone tunnel in rabbits, Acta Biomater 63 (2017) 393-410.

[15] S. Yoshizawa, A. Brown, A. Barchowsky, C. Sfeir, Magnesium ion stimulation of bone marrow stromal cells enhances osteogenic activity, simulating the effect of magnesium alloy degradation, Acta Biomater 10(6) (2014) 2834-42.

[16] R.C. Ransom, A.C. Carter, A. Salhotra, T. Leavitt, O. Marecic, M.P. Murphy, M.L. Lopez, Y.N. Wei, C.D. Marshall, E.Z. Shen, R.E. Jones, A. Sharir, O.D. Klein, C.K.F. Chan, D.C. Wan, H.Y. Chang, M.T. Longaker, Mechanoresponsive stem cells acquire neural crest fate in jaw regeneration, Nature 563(7732) (2018) 514-+.

[17] F. Witte, V. Kaese, H. Haferkamp, E. Switzer, A. Meyer-Lindenberg, C.J. Wirth, H. Windhagen, In vivo corrosion of four magnesium alloys and the associated bone response, Biomaterials 26(17) (2005) 3557-63.

[18] J. Zhang, S. Hiromoto, T. Yamazaki, H. Huang, G. Jia, H. Li, G. Yuan, Macrophage phagocytosis of biomedical Mg alloy degradation products prepared by electrochemical method, Mater Sci Eng C Mater Biol Appl 75 (2017) 1178-1183.

[19] S. Remennik, I. Bartsch, E. Willbold, F. Witte, D. Shechtman, New, fast corroding high ductility Mg–Bi–Ca and Mg–Bi–Si alloys, with no clinically observable gas formation in bone implants, Materials Science and Engineering: B 176(20) (2011) 1653-1659.

[20] W. Xu, N. Birbilis, G. Sha, Y. Wang, J.E. Daniels, Y. Xiao, M. Ferry, A

high-specific-strength and corrosion-resistant magnesium alloy, Nat Mater 14(12) (2015) 1229-35.

[21] M.B. Kannan, Electrochemical deposition of calcium phosphates on magnesium and its alloys for improved biodegradation performance: A review, Surface and Coatings Technology 301 (2016) 36-41.

[22] L. Li, M. Zhang, Y. Li, J. Zhao, L. Qin, Y. Lai, Corrosion and biocompatibility improvement of magnesium-based alloys as bone implant materials: a review, Regenerative Biomaterials 4(2) (2017) 129-137.

[23] Y.F. Zheng, X.N. Gu, F. Witte, Biodegradable metals, Materials Science and Engineering: R: Reports 77 (2014) 1-34.

[24] S.D. Cramer, B.S. Covino Jr, C. Moosbrugger, B.R. Sanders, G.J. Anton, N. Hrivnak, J. Kinson, C. Polakowski, K. Muldoon, S.D. Henry, ASM handbook, ASM international Materials Park, Ohio2003.

[25] L.Y. Li, L.Y. Cui, R.C. Zeng, S.Q. Li, X.B. Chen, Y. Zheng, M.B. Kannan, Advances in functionalized polymer coatings on biodegradable magnesium alloys - A review, Acta Biomater 79 (2018) 23-36.

[26] G. Song, Control of biodegradation of biocompatable magnesium alloys, Corrosion science 49(4) (2007) 1696-1701.

[27] A. Atrens, G.-L. Song, F. Cao, Z. Shi, P.K. Bowen, Advances in Mg corrosion and research suggestions, Journal of Magnesium and Alloys 1(3) (2013) 177-200.

[28] H.-D. Jung, H. Sun Park, M.-H. Kang, S.-M. Lee, H.-E. Kim, Y. Estrin, Y.-H. Koh, Polyetheretherketone/magnesium composite selectively coated with hydroxyapatite for enhanced in vitro bio-corrosion resistance and biocompatibility, Materials Letters 116 (2014) 20-22.

[29] Q.-S. Yao, F. Zhang, L. Song, R.-C. Zeng, L.-Y. Cui, S.-Q. Li, Z.-L. Wang, E.-H. Han, Corrosion resistance of a ceria/polymethyltrimethoxysilane modified Mg-Al-layered double hydroxide on AZ31 magnesium alloy, Journal of Alloys and Compounds 764 (2018) 913-928.

[30] Y.F. Ding, C.E. Wen, P. Hodgson, Y.C. Li, Effects of alloying elements on the corrosion behavior and biocompatibility of biodegradable magnesium alloys: a review, J Mater Chem B 2(14) (2014) 1912-1933.

[31] C.Q. Li, D.K. Xu, B.J. Wang, L.Y. Sheng, E.H. Han, Suppressing Effect of Heat TreatMent on the Portevin-Le Chatelier Phenomenon of Mg-4%Li-6%Zn-1.2%Y Alloy, J Mater Sci Technol 32(12) (2016) 1232-1238.

[32] H. Hornberger, S. Virtanen, A.R. Boccaccini, Biomedical coatings on magnesium alloys - a review, Acta Biomater 8(7) (2012) 2442-55.

[33] L. Xu, F. Pan, G. Yu, L. Yang, E. Zhang, K. Yang, In vitro and in vivo evaluation of the surface bioactivity of a calcium phosphate coated magnesium alloy, Biomaterials 30(8) (2009) 1512-23.

[34] Y. Zhang, G. Zhang, M. Wei, Controlling the biodegradation rate of magnesium using biomimetic apatite coating, J Biomed Mater Res B Appl

Biomater 89(2) (2009) 408-14.

[35] M.B. Kannan, R.S. Raman, In vitro degradation and mechanical integrity of calcium-containing magnesium alloys in modified-simulated body fluid, Biomaterials 29(15) (2008) 2306-2314.

[36] S. Shadanbaz, G.J. Dias, Calcium phosphate coatings on magnesium alloys for biomedical applications: a review, Acta Biomater 8(1) (2012) 20-30.

[37] S. Hiromoto, M. Tomozawa, Corrosion Behavior of Magnesium with Hydroxyapatite Coatings Formed by Hydrothermal Treatment, Mater Trans 51(11) (2010) 2080-2087.

[38] J. Yang, F. Cui, Q. Yin, Y. Zhang, T. Zhang, X. Wang, Characterization and degradation study of calcium phosphate coating on magnesium alloy bone implant in vitro, IEEE Transactions on plasma science 37(7) (2009) 1161-1168.

[39] Y.W. Song, D.Y. Shan, E.H. Han, Electrodeposition of hydroxyapatite coating on AZ91D magnesium alloy for biomaterial application, Materials Letters 62(17-18) (2008) 3276-3279.

[40] K.Y. Chiu, M.H. Wong, F.T. Cheng, H.C. Man, Characterization and corrosion studies of fluoride conversion coating on degradable Mg implants, Surf Coat Tech 202(3) (2007) 590-598.

[41] F. Witte, J. Fischer, J. Nellesen, C. Vogt, J. Vogt, T. Donath, F. Beckmann, In vivo corrosion and corrosion protection of magnesium alloy LAE442, Acta Biomaterialia 6(5) (2010) 1792-1799.

[42] P.B. Srinivasan, J. Liang, C. Blawert, M. Stormer, W. Dietzel, Characterization of calcium containing plasma electrolytic oxidation coatings on AM50 magnesium alloy, Appl Surf Sci 256(12) (2010) 4017-4022.

[43] C.-C. Chen, J.-Y. Chueh, H. Tseng, H.-M. Huang, S.-Y. Lee, Preparation and characterization of biodegradable PLA polymeric blends, Biomaterials 24(7) (2003) 1167-1173.

[44] J. Blacklock, T.K. Sievers, H. Handa, Y.Z. You, D. Oupicky, G.Z. Mao, H. Mohwald, Cross-Linked Bioreducible Layer-by-Layer Films for Increased Cell Adhesion and Transgene Expression, J Phys Chem B 114(16) (2010) 5283-5291.

[45] J. Li, P. Cao, X. Zhang, S. Zhang, Y. He, In vitro degradation and cell attachment of a PLGA coated biodegradable Mg–6Zn based alloy, Journal of materials science 45(22) (2010) 6038-6045.

[46] J.Y. Chen, X.B. Chen, J.L. Li, B. Tang, N. Birbilis, X.G. Wang, Electrosprayed PLGA smart containers for active anti-corrosion coating on magnesium alloy AMlite, J Mater Chem A 2(16) (2014) 5738-5743.

[47] H.M. Wong, K.W.K. Yeung, K.O. Lam, V. Tam, P.K. Chu, K.D.K. Luk, K.M.C. Cheung, A biodegradable polymer-based coating to control the performance of magnesium alloy orthopaedic implants, Biomaterials 31(8) (2010) 2084-2096.

[48] D. Mushahary, C. Wen, J.M. Kumar, J. Lin, N. Harishankar, P. Hodgson,

G. Pande, Y. Li, Collagen type-I leads to in vivo matrix mineralization and secondary stabilization of Mg–Zr–Ca alloy implants, Colloids and Surfaces B: Biointerfaces 122 (2014) 719-728.

[49] S. Agarwal, J. Curtin, B. Duffy, S. Jaiswal, Biodegradable magnesium alloys for orthopaedic applications: A review on corrosion, biocompatibility and surface modifications, Mater Sci Eng C Mater Biol Appl 68 (2016) 948-963.

[50] D.R. Sumner, Long-term implant fixation and stress-shielding in total hip replacement, J Biomech 48(5) (2015) 797-800.

[51] Y. Noyama, T. Miura, T. Ishimoto, T. Itaya, M. Niinomi, T. Nakano, Bone Loss and Reduced Bone Quality of the Human Femur after Total Hip Arthroplasty under Stress-Shielding Effects by Titanium-Based Implant, Mater Trans 53(3) (2012) 565-570.

[52] D.V. Andreeva, D. Fix, H. Mohwald, D.G. Shchukin, Self-Healing Anticorrosion Coatings Based on pH-Sensitive Polyelectrolyte/Inhibitor Sandwichlike Nanostructures, Adv Mater 20(14) (2008) 2789-94.

[53] J. Hiller, J.D. Mendelsohn, M.F. Rubner, Reversibly erasable nanoporous anti-reflection coatings from polyelectrolyte multilayers, Nat Mater 1(1) (2002) 59-63.

[54] N.J. Shah, J. Hong, M.N. Hyder, P.T. Hammond, Osteophilic multilayer coatings for accelerated bone tissue growth, Adv Mater 24(11) (2012) 1445-50.

[55] W.H. Song, Y.K. Jun, Y. Han, S.H. Hong, Biomimetic apatite coatings on micro-arc oxidized titania, Biomaterials 25(17) (2004) 3341-9.

[56] M.A. Stuart, W.T. Huck, J. Genzer, M. Muller, C. Ober, M. Stamm, G.B. Sukhorukov, I. Szleifer, V.V. Tsukruk, M. Urban, F. Winnik, S. Zauscher, I. Luzinov, S. Minko, Emerging applications of stimuli-responsive polymer materials, Nat Mater 9(2) (2010) 101-13.

[57] Q. Wei, T. Becherer, P.L. Noeske, I. Grunwald, R. Haag, A universal approach to crosslinked hierarchical polymer multilayers as stable and highly effective antifouling coatings, Adv Mater 26(17) (2014) 2688-93, 2615.

[58] R.H. Kim, D.H. Kim, J. Xiao, B.H. Kim, S.I. Park, B. Panilaitis, R. Ghaffari, J. Yao, M. Li, Z. Liu, V. Malyarchuk, D.G. Kim, A.P. Le, R.G. Nuzzo, D.L. Kaplan, F.G. Omenetto, Y. Huang, Z. Kang, J.A. Rogers, Waterproof AlInGaP optoelectronics on stretchable substrates with applications in biomedicine and robotics, Nat Mater 9(11) (2010) 929-37.

[59] Z. Liu, X. Wang, D. Qi, C. Xu, J. Yu, Y. Liu, Y. Jiang, B. Liedberg, X. Chen, High-Adhesion Stretchable Electrodes Based on Nanopile Interlocking, Adv Mater 29(2) (2017).

[60] Z. Song, T. Ma, R. Tang, Q. Cheng, X. Wang, D. Krishnaraju, R. Panat, C.K. Chan, H. Yu, H. Jiang, Origami lithium-ion batteries, Nat Commun 5 (2014) 3140.

[61] R. Seghir, S. Arscott, Controlled mud-crack patterning and self-organized

cracking of polydimethylsiloxane elastomer surfaces, Sci Rep 5 (2015) 14787.

[62] J. Lee, T.J. Ha, H.F. Li, K.N. Parrish, M. Holt, A. Dodabalapur, R.S. Ruoff, D. Akinwande, 25 GHz Embedded-Gate Graphene Transistors with High-K Dielectrics on Extremely Flexible Plastic Sheets, Acs Nano 7(9) (2013) 7744-7750.

[63] C. Peng, Z. Jia, H. Neilson, T. Li, J. Lou, In Situ Electro-Mechanical Experiments and Mechanics Modeling of Fracture in Indium Tin Oxide-Based Multilayer Electrodes, Advanced Engineering Materials 15(4) (2013) 250-256.

[64] K. Efimenko, M. Rackaitis, E. Manias, A. Vaziri, L. Mahadevan, J. Genzer, Nested self-similar wrinkling patterns in skins, Nat Mater 4(4) (2005) 293-7.

[65] D.Y. Khang, H.Q. Jiang, Y. Huang, J.A. Rogers, A stretchable form of single-crystal silicon for high-performance electronics on rubber substrates, Science 311(5758) (2006) 208-212.

[66] S.J. Li, M. Niinomi, T. Akahori, T. Kasuga, R. Yang, Y.L. Hao, Fatigue characteristics of bioactive glass-ceramic-coated Ti-29Nb-13Ta-4.6Zr for biomedical application, Biomaterials 25(17) (2004) 3369-78.

[67] G. Wu, J.M. Ibrahim, P.K. Chu, Surface design of biodegradable magnesium alloys — A review, Surface and Coatings Technology 233 (2013) 2-12.

[68] A.H. Martinez Sanchez, B.J. Luthringer, F. Feyerabend, R. Willumeit, Mg and Mg alloys: how comparable are in vitro and in vivo corrosion rates? A

review, Acta Biomater 13 (2015) 16-31.

[69] J. Walker, S. Shadanbaz, T.B. Woodfield, M.P. Staiger, G.J. Dias, Magnesium biomaterials for orthopedic application: a review from a biological perspective, J Biomed Mater Res B Appl Biomater 102(6) (2014) 1316-31.

[70] M.P. Staiger, A.M. Pietak, J. Huadmai, G. Dias, Magnesium and its alloys as orthopedic biomaterials: a review, Biomaterials 27(9) (2006) 1728-34.

[71] R.-G. Hu, S. Zhang, J.-F. Bu, C.-J. Lin, G.-L. Song, Recent progress in corrosion protection of magnesium alloys by organic coatings, Progress in Organic Coatings 73(2-3) (2012) 129-141.

[72] C.L. Liu, J. Jiang, M. Wang, Y.J. Wang, P.K. Chu, W.J. Huang, In Vitro Degradation and Biocompatibility of WE43, ZK60, and AZ91 Biodegradable Magnesium Alloys, Advanced Materials Research 287-290 (2011) 2008-2014.

[73] W. Jin, G. Wu, H. Feng, W. Wang, X. Zhang, P.K. Chu, Improvement of corrosion resistance and biocompatibility of rare-earth WE43 magnesium alloy by neodymium self-ion implantation, Corrosion Science 94 (2015) 142-155.

[74] L. Xu, G. Yu, E. Zhang, F. Pan, K. Yang, In vivo corrosion behavior of Mg-Mn-Zn alloy for bone implant application, J Biomed Mater Res A 83(3) (2007) 703-11.

[75] J.H. Jo, B.G. Kang, K.S. Shin, H.E. Kim, B.D. Hahn, D.S. Park, Y.H. Koh, Hydroxyapatite coating on magnesium with MgF(2) interlayer for enhanced

corrosion resistance and biocompatibility, J Mater Sci Mater Med 22(11) (2011) 2437-47.

[76] L. Li, J. Gao, Y. Wang, Evaluation of cyto-toxicity and corrosion behavior of alkali-heat-treated magnesium in simulated body fluid, Surface and Coatings Technology 185(1) (2004) 92-98.

[77] J.N. Li, P. Cao, X.N. Zhang, S.X. Zhang, Y.H. He, In vitro degradation and cell attachment of a PLGA coated biodegradable Mg–6Zn based alloy, Journal of Materials Science 45(22) (2010) 6038-6045.

[78] H.M. Wong, K.W. Yeung, K.O. Lam, V. Tam, P.K. Chu, K.D. Luk, K.M. Cheung, A biodegradable polymer-based coating to control the performance of magnesium alloy orthopaedic implants, Biomaterials 31(8) (2010) 2084-96.

[79] L. Xu, A. Yamamoto, Characteristics and cytocompatibility of biodegradable polymer film on magnesium by spin coating, Colloids Surf B Biointerfaces 93 (2012) 67-74.

[80] S.B. Kim, J.H. Jo, S.M. Lee, H.E. Kim, K.H. Shin, Y.H. Koh, Use of a poly(ether imide) coating to improve corrosion resistance and biocompatibility of magnesium (Mg) implant for orthopedic applications, J Biomed Mater Res A 101(6) (2013) 1708-15.

[81] S.V. Dorozhkin, Calcium orthophosphate coatings on magnesium and its biodegradable alloys, Acta Biomater 10(7) (2014) 2919-34.

[82] R. Narayanan, S.K. Seshadri, T.Y. Kwon, K.H. Kim, Calcium phosphate-

based coatings on titanium and its alloys, J Biomed Mater Res B Appl Biomater 85(1) (2008) 279-99.

[83] S.R. Paital, N.B. Dahotre, Calcium phosphate coatings for bio-implant applications: Materials, performance factors, and methodologies, Materials Science and Engineering: R: Reports 66(1-3) (2009) 1-70.

[84] J.H. Jo, Y. Li, S.M. Kim, H.E. Kim, Y.H. Koh, Hydroxyapatite/poly(epsilon-caprolactone) double coating on magnesium for enhanced corrosion resistance and coating flexibility, J Biomater Appl 28(4) (2013) 617-25.

[85] J. Du, J.H. Lee, A.T. Jang, A. Gu, M. Hossaini-Zadeh, R. Prevost, D.A. Curtis, S.P. Ho, Biomechanics and strain mapping in bone as related to immediately-loaded dental implants, J Biomech 48(12) (2015) 3486-94.

[86] J. Du, J.H. Lee, A.T. Jang, A. Gu, M. Hossaini-Zadeh, R. Prevost, D.A. Curtis, S.P. Ho, Biomechanics and strain mapping in bone as related to immediately-loaded dental implants, J Biomech 48(12) (2015) 3486-3494.

[87] J.-W. Wang, B. Li, Y.-P. Cao, X.-Q. Feng, Surface Wrinkling Patterns of Film–Substrate Systems With a Structured Interface, Journal of Applied Mechanics 82(5) (2015) 051009.

[88] A. Dey, A.K. Mukhopadhyay, Fracture Toughness of Microplasma-Sprayed Hydroxyapatite Coating by Nanoindentation, International Journal of Applied Ceramic Technology 8(3) (2011) 572-590.

[89] S.M. Kim, J.H. Jo, S.M. Lee, M.H. Kang, H.E. Kim, Y. Estrin, J.H. Lee, J.W. Lee, Y.H. Koh, Hydroxyapatite-coated magnesium implants with improved in vitro and in vivo biocorrosion, biocompatibility, and bone response, Journal of Biomedical Materials Research Part A 102(2) (2014) 429-441.

[90] T. Kokubo, H. Takadama, How useful is SBF in predicting in vivo bone bioactivity?, Biomaterials 27(15) (2006) 2907-2915.

[91] H. Somekawa, T. Mukai, Effect of grain refinement on fracture toughness in extruded pure magnesium, Scripta Materialia 53(9) (2005) 1059-1064.

[92] X.-N. Gu, S.-S. Li, X.-M. Li, Y.-B. Fan, Magnesium based degradable biomaterials: A review, Frontiers of Materials Science 8(3) (2014) 200-218.

[93] M. Diez, M.H. Kang, S.M. Kim, H.E. Kim, J. Song, Hydroxyapatite (HA)/poly-L-lactic acid (PLLA) dual coating on magnesium alloy under deformation for biomedical applications, J Mater Sci Mater Med 27(2) (2016) 34.

[94] K. Anselme, Osteoblast adhesion on biomaterials, Biomaterials 21(7) (2000) 667-681.

[95] A. Curtis, C. Wilkinson, Topographical control of cells, Biomaterials 18(24) (1997) 1573-1583.

[96] G. Fu, W.O. Soboyejo, Cell/surface interactions of human osteo-sarcoma (HOS) cells and micro-patterned polydimelthylsiloxane (PDMS) surfaces, Mat Sci Eng C-Mater 29(6) (2009) 2011-2018.

[97] J. Hu, C. Hardy, C.M. Chen, S. Yang, A.S. Voloshin, Y.L. Liu, Enhanced Cell Adhesion and Alignment on Micro-Wavy Patterned Surfaces, Plos One 9(8) (2014).

[98] H. Sunami, I. Yokota, Y. Igarashi, Influence of the pattern size of micropatterned scaffolds on cell morphology, proliferation, migration and F-actin expression, Biomater Sci-Uk 2(3) (2014) 399-409.

[99] M.H. Lee, N. Oh, S.W. Lee, R. Leesungbok, S.E. Kim, Y.P. Yun, J.H. Kang, Factors influencing osteoblast maturation on microgrooved titanium substrata, Biomaterials 31(14) (2010) 3804-15.

[100] J.C. Middleton, A.J. Tipton, Synthetic biodegradable polymers as orthopedic devices, Biomaterials 21(23) (2000) 2335-2346.

[101] M. Rahim, S. Ullah, P. Mueller, Advances and Challenges of Biodegradable Implant Materials with a Focus on Magnesium-Alloys and Bacterial Infections, Metals 8(7) (2018).

[102] N. Li, Y. Zheng, Novel Magnesium Alloys Developed for Biomedical Application: A Review, Journal of Materials Science & Technology 29(6) (2013) 489-502.

[103] F. Witte, J. Fischer, J. Nellesen, H.A. Crostack, V. Kaese, A. Pisch, F. Beckmann, H. Windhagen, In vitro and in vivo corrosion measurements of magnesium alloys, Biomaterials 27(7) (2006) 1013-8.

[104] D. Zang, R. Zhu, W. Zhang, X. Yu, L. Lin, X. Guo, M. Liu, L. Jiang,

Corrosion-Resistant Superhydrophobic Coatings on Mg Alloy Surfaces Inspired by Lotus Seedpod, Advanced Functional Materials 27(8) (2017).

[105] K.-H. Cheon, C. Gao, M.-H. Kang, H.-D. Jung, T.-S. Jang, H.-E. Kim, Y. Li, J. Song, A crack-free anti-corrosive coating strategy for magnesium implants under deformation, Corrosion Science 132 (2018) 116-124.

[106] T.F. Conceicao, N. Scharnagl, C. Blawert, W. Dietzel, K.U. Kainer, Corrosion protection of magnesium alloy AZ31 sheets by spin coating process with poly(ether imide) [PEI], Corrosion Science 52(6) (2010) 2066-2079.

[107] T.F. da Conceicao, N. Scharnagl, W. Dietzel, K.U. Kainer, Corrosion protection of magnesium AZ31 alloy using poly(ether imide) [PEI] coatings prepared by the dip coating method: Influence of solvent and substrate pre-treatment, Corrosion Science 53(1) (2011) 338-346.

[108] M.H. Kang, T.S. Jang, H.D. Jung, S.M. Kim, H.E. Kim, Y.H. Koh, J. Song, Poly(ether imide)-silica hybrid coatings for tunable corrosion behavior and improved biocompatibility of magnesium implants, Biomed Mater 11(3) (2016) 035003.

[109] A. Zomorodian, M.P. Garcia, T. Moura e Silva, J.C. Fernandes, M.H. Fernandes, M.F. Montemor, Corrosion resistance of a composite polymeric coating applied on biodegradable AZ31 magnesium alloy, Acta Biomater 9(10) (2013) 8660-70.

[110] C. Park, Y.J. Seong, I.G. Kang, E.H. Song, H. Lee, J. Kim, H.D. Jung,

H.E. Kim, T.S. Jang, Enhanced Osseointegration Ability of Poly(lactic acid) via Tantalum Sputtering-Based Plasma Immersion Ion Implantation, ACS Appl Mater Interfaces 11(11) (2019) 10492-10504.

[111] C. Park, S.W. Lee, J. Kim, E.H. Song, H.D. Jung, J.U. Park, H.E. Kim, S. Kim, T.S. Jang, Reduced fibrous capsule formation at nano-engineered silicone surfaces via tantalum ion implantation, Biomater Sci 7(7) (2019) 2907-2919.

[112] D. Mareci, R. Chelariu, D.M. Gordin, G. Ungureanu, T. Gloriant, Comparative corrosion study of Ti-Ta alloys for dental applications, Acta Biomater 5(9) (2009) 3625-39.

[113] B.R. Levine, S. Sporer, R.A. Poggie, C.J. Della Valle, J.J. Jacobs, Experimental and clinical performance of porous tantalum in orthopedic surgery, Biomaterials 27(27) (2006) 4671-81.

[114] M.H. Kang, H. Lee, T.S. Jang, Y.J. Seong, H.E. Kim, Y.H. Koh, J. Song, H.D. Jung, Biomimetic porous Mg with tunable mechanical properties and biodegradation rates for bone regeneration, Acta Biomater 84 (2019) 453-467.

[115] I.G. Kang, C.I. Park, H. Lee, H.E. Kim, S.M. Lee, Hydroxyapatite Microspheres as an Additive to Enhance Radiopacity, Biocompatibility, and Osteoconductivity of Poly(methyl methacrylate) Bone Cement, Materials (Basel) 11(2) (2018).

[116] D.Y. Shin, M.H. Kang, I.G. Kang, H.E. Kim, S.H. Jeong, In vitro and in vivo evaluation of polylactic acid-based composite with tricalcium phosphate

microsphere for enhanced biodegradability and osseointegration, J Biomater Appl 32(10) (2018) 1360-1370.

[117] E. Atanassova, T. Dimitrova, J. Koprinarova, Aes and Xps Study of Thin Rf-Sputtered Ta2o5 Layers, Appl Surf Sci 84(2) (1995) 193-202.

[118] J.Y. Zhang, I.W. Boyd, Thin tantalum and tantalum oxide films grown by pulsed laser deposition, Appl Surf Sci 168(1-4) (2000) 234-238.

[119] M. Grujicic, V. Sellappan, M.A. Omar, N. Seyr, A. Obieglo, M. Erdmann, J. Holzleitner, An overview of the polymer-to-metal direct-adhesion hybrid technologies for load-bearing automotive components, Journal of Materials Processing Technology 197(1-3) (2008) 363-373.

[120] W. Jin, G. Wang, Z. Lin, H. Feng, W. Li, X. Peng, A.M. Qasim, P.K. Chu, Corrosion resistance and cytocompatibility of tantalum-surface-functionalized biomedical ZK60 Mg alloy, Corrosion Science 114 (2017) 45-56.

[121] D.Y. Zhang, Q.Y. Fei, H.M. Zhao, M. Geng, X.C. Zeng, P.K. Chu, Effects of tantalum ion implantation on the surface properties of Al–Mg alloy, Thin Solid Films 484(1-2) (2005) 215-218.

[122] X. Wang, X. Zeng, G. Wu, S. Yao, Y. Lai, Effects of tantalum ion implantation on the corrosion behavior of AZ31 magnesium alloys, Journal of Alloys and Compounds 437(1-2) (2007) 87-92.

[123] P. Tian, X. Liu, Surface modification of biodegradable magnesium and its alloys for biomedical applications, Regen Biomater 2(2) (2015) 135-51.

[124] P.K. Mattila, P. Lappalainen, Filopodia: molecular architecture and cellular functions, Nat Rev Mol Cell Biol 9(6) (2008) 446-54.

[125] U. Meyer, A. Büchter, H.P. Wiesmann, U. Joos, D.B. Jones, Basic reactions of osteoblasts on structured material surfaces, European Cells and Materials 9 (2005) 39-49.

[126] S.A. Redey, M. Nardin, D. Bernache-Assolant, C. Rey, P. Delannoy, L. Sedel, P.J. Marie, Behavior of human osteoblastic cells on stoichiometric hydroxyapatite and type A carbonate apatite: Role of surface energy, J Biomed Mater Res 50(3) (2000) 353-364.

[127] B.S. Moon, S. Kim, H.E. Kim, T.S. Jang, Hierarchical micro-nano structured Ti6Al4V surface topography via two-step etching process for enhanced hydrophilicity and osteoblastic responses, Mater Sci Eng C Mater Biol Appl 73 (2017) 90-98.

[128] T. Groth, G. Altankov, Studies on cell-biomaterial interaction role of tyrosine phosphorylation during fibroblast spreading on surfaces varying in wettability, Biomaterials 17(12) (1996) 1227-1234.

[129] S.H. Jun, E.J. Lee, S.W. Yook, H.E. Kim, H.W. Kim, Y.H. Koh, A bioactive coating of a silica xerogel/chitosan hybrid on titanium by a room temperature sol-gel process, Acta Biomater 6(1) (2010) 302-7.

[130] T.S. Jang, E.J. Lee, J.H. Jo, J.M. Jeon, M.Y. Kim, H.E. Kim, Y.H. Koh, Fibrous membrane of nano-hybrid poly-L-lactic acid/silica xerogel for guided

bone regeneration, J Biomed Mater Res B Appl Biomater 100(2) (2012) 321-30.

[131] V.K. Balla, S. Banerjee, S. Bose, A. Bandyopadhyay, Direct laser processing of a tantalum coating on titanium for bone replacement structures, Acta Biomater 6(6) (2010) 2329-34.

[132] C.M. Serre, M. Papillard, P. Chavassieux, J.C. Voegel, G. Boivin, Influence of magnesium substitution on a collagen–apatite biomaterial on the production of a calcifying matrix by human osteoblasts, J Biomed Mater Res 42(4) (1998) 626-633.

[133] A. Abdal-hay, N.A.M. Barakat, J.K. Lim, Hydroxyapatite-doped poly(lactic acid) porous film coating for enhanced bioactivity and corrosion behavior of AZ31 Mg alloy for orthopedic applications, Ceramics International 39(1) (2013) 183-195.

[134] M. Padial-Molina, P. Galindo-Moreno, J.E. Fernandez-Barbero, F. O'Valle, A.B. Jodar-Reyes, J.L. Ortega-Vinuesa, P.J. Ramon-Torregrosa, Role of wettability and nanoroughness on interactions between osteoblast and modified silicon surfaces, Acta Biomater 7(2) (2011) 771-8.

Abstract (Korean)

국문 초록

생분해성 마그네슘 임플란트의 기능성 표면 처리를 통한 부식 저항성 및 생체 활성도 향상

서울대학교

재료공학부

천 광 희

전 세계적으로 마그네슘 (Mg) 과 그 합금은 생분해성 재료에 대한 수요가 증가함에 따라 생체 재료 분야에서 광범위하게 연구되어 오고 있다. 마그네슘은 체내에서 독성 부산물 없이 분해되며 식립체의 용해와 조직 재생이 동시에 일어난다는 장점이 있어 추가적인 2 차 제거 수술이 필요하지 않다고 알려져 있다. 또한, 다른 금속 임플란트 중에서 인간의 뼈와 가장 유사한 기계적

특성을 지니고 있어 '응력 차폐 효과'가 억제된다. 그러나 우수한 장점에도 불구하고, 마그네슘의 낮은 부식 저항성으로 인해 실제 생체 재료 분야에서의 활용이 제한되고 있다. 따라서, 마그네슘의 내부식성 및 생체 적합성을 향상시키기 위한 표면 처리에 대한 연구가 활발하게 진행되어 오고 있다. 본 연구에서는 실제 의료 환경에서 재료에 가해지는 변형을 고려하여 마그네슘 표면에 기능성 표면 처리에 대한 연구를 수행하여 마그네슘 재료의 부식 저항성 및 생체 적합성을 향상시켰다.

첫 번째 연구에서는 마그네슘 표면에 곡선 모양의 그루브 패턴을 도입하여 변형에도 견딜 수 있는 하이드록시아파타이트-폴리에테르이미드 하이브리드 코팅층을 개발하였다. 일반적으로 마그네슘 재료의 부식 저항성을 높이기 위해 높은 부식 저항성을 가진 세라믹 코팅층에 관한 연구가 활발히 진행되어 왔다. 하지만 세라믹 코팅층은 변형이 가해지면 균열이나 박리 등의 결함이 발생하게 되고 이로 인하여 부식 저항성과 생체 적합성을 유지하지 못한다는 단점이 있다. 이러한 결함 발생을 억제하기 위해 마그네슘 표면에 마이크로 단위의 그루브 패턴을 도입하여 스트레인 분포를 형상에 맞게 제어하였다. 적절한 패턴의 크기를 결정하기 위해 유한 요소

해석 (Finite element analysis, FEA)를 활용하여 스트레인의 재분포를 확인함과 동시에 결함으로 작용하지 않도록 그루브의 크기를 결정하였다. 결정된 그루브 패턴을 마그네슘 표면에 레이저 가공으로 제작한 후 밸리 파트에는 폴리에테르이미드를, 그루브의 힐 파트에는 하이드록시아파타이트를 선택적으로 코팅함으로써 변형에도 형태를 유지할 수 있는 하이드록시아파타이트-폴리에테르이미드 하이브리드 코팅층을 완성하였다. 완성된 코팅층은 기존 하이드록시아파타이트만 코팅된 마그네슘과는 다르게 변형이 가해지더라도 코팅층에 결함이 발생하지 않고 코팅층의 형상과 우수한 부식 저항성 및 생체적합성이 유지되는 것을 확인할 수 있었다. 따라서 그루브 패턴이 도입된 하이드록시아파타이트-폴리에테르이미드 코팅층은 인장 혹은 굽힘 변형이 발생하는 정형외과용 스캐폴드로 활용될 수 있는 잠재력을 지니고 있음을 확인할 수 있었다.

두 번째 연구에서는 마그네슘에 코팅된 고분자 코팅층으로 탄탈륨 금속 이온을 주입함으로써 훨씬 더 많은 변형에도 안정적으로 부식 저항성과 생체 적합성을 크게 향상시키는 탄탈륨-폴리에테르이미드 코팅층에 관한 연구를 진행하였다. 실제 마그네슘의 부식 저항성을 향상시키기 위해서 표면에 고분자 코팅을 많이 진행되지

만 대부분의 합성 고분자 코팅층은 그 생체 적합성이 낮다고 알려져 있다. 따라서 이를 해결하고자 스퍼터링 공정을 통해 생체활성도가 높은 금속 이온을 주입하여 고분자 코팅층의 표면을 생체친화적으로 개질하였다. 마그네슘 표면에 폴리에테르이미드 고분자를 먼저 코팅한 후 스퍼터링 기술을 이용한 금속 이온 주입 공정을 약 30초간 진행하여 탄탈륨 금속 이온을 주입하였다. 스퍼터링 기반 금속 이온 주입 공정 후 고분자 코팅층에는 특별한 결함과 계면 없이 고분자 코팅층 표면에 약 10㎚ 두께의 탄탈륨 주입층이 형성되어 있음을 확인하였다. 또한, 주입된 탄탈륨은 기존 폴리에테르이미드 코팅층과 특별한 계면을 형성하지 않기 때문에 10%의 인장 변형이 가해지더라도 그 표면 형상을 유지하고 있었음을 확인하였다. 또한, 코팅 되지 않은 마그네슘에 비해 부식 속도가 크게 감소하였으며 주입된 탄탈륨으로 인해 고분자 코팅층 표면의 생체적합성이 크게 향상되어 조골모세포와의 친화성 및 골 유착능이 상당히 증가하였음을 확인하였다.

결과적으로 본 연구는 마그네슘이 가지고 있는 높은 부식성을 억제하며 생체적합성을 향상시키기위한 기능성 표면 개질을 제안하였다. 마그네슘 표면에 하이드록시아파타이트-폴리에테르이미

드 코팅 및 탄탈륨/폴리에테르이미드 코팅을 도입함으로써 다양한 기계적 변형에서 향상된 내부식성과 생체적합성을 나타내어 마그네슘 기반의 생분해성 임플란트의 잠재력을 확인하였다.

주요어: 마그네슘; 표면 코팅; 부식 저항성; 유한 요소 해석; 패터닝; 하이드록시아파타이트; 폴리에테르이미드; 탄탈륨; 생분해성 스캐폴드;

학번: 2014-21455